Novel Amphiphilic Probes for [^{18}F]-Radiolabeling Preformed Liposomes and Determination of Liposomal Trafficking by Positron Emission Tomography

Takeo Urakami,[†] Shuji Akai,[‡] Yurie Katayama,[†] Norihiro Harada,[§] Hideo Tsukada,[§] and Naoto Oku*[,†]

Department of Medical Biochemistry and Global COE and Department of Synthetic Organic Chemistry, Graduate School of Pharmaceutical Sciences, University of Shizuoka, Yada, Suruga-ku, Shizuoka 422-8526, Japan, and PET Center, Central Research Laboratory, Hamamatsu Photonics K.K., Hirakuchi, Hamakita-ku, Hamamatsu 434-8601, Japan

Received August 24, 2007

Abstract: Positron-emission tomography (PET) is a noninvasive real-time functional imaging system and is expected to be useful for the development of new drug candidates in clinical trials. For its application with preformulated liposomes, we devised an optimized [^{18}F]-compound and developed a direct liposome modification method that we termed the "solid-phase transition method". We were successful in using 1-[^{18}F]fluoro-3,6-dioxatetracosane ([^{18}F]**7a**) for in vivo trafficking of liposomes. This method might be a useful tool in preclinical and clinical studies of lipidic particle-related drugs.

Liposomes can be used as multipurpose drug carriers in a wide range of applications. Liposomes have been used as one of the most ideal drug carriers for anticancer agents, antifungal antibiotics, photosensitizers, nucleic acid derivatives for gene therapy, and so on.[1–4] From the viewpoint of drug delivery systems (DDSs[a]) the pharmacokinetics, pharmacodynamics, and pharmacotoxics of such drugs have been improved through the formulation of liposomes or other kinds of lipidic particles such as lipid complexes and microspheres. To use liposomes as drug carriers, it is necessary to consider many properties of liposomal formulations, e.g., lipid composition, vesicular size, surface electrostatic potential, and functional modification, that influence independently or mutually the pharmacological characteristics of the liposomes.[5] Comprehensive evaluation of liposomes in the living body is therefore important for the development of liposomal DDS drugs and in DDS studies. For evaluation of the pharmacokinetics of liposomes in vivo, noninvasive real-time imaging of liposomes is one of the ideal techniques.

Positron emission tomography is a noninvasive technique and has been used for the clinical functional diagnosis in many applications related to oncology, neurology, cardiology, psychiatry, and so on.[6,7] Also, this technique can be applied in preclinical studies. Once a positron-labeled candidate drug is injected into animals, the distribution of the drug in the body, the tissues in which it becomes concentrated, and its eventual elimination can be monitored far more quickly and cost effectively than by the older invasive techniques of killing and dissecting the animals to obtain similar information.[8] In this study, we applied this idea to DDS drugs.

We previously reported the methodology for detecting noninvasive liposomal trafficking by PET.[9,10] In those studies, we used a water-soluble compound, [2-^{18}F]2-deoxy-2-fluoroglucose ([^{18}F]FDG), encapsulated inside the vesicles. To encapsulate the [^{18}F]FDG, we restructured the lipid bilayer by repeating freeze–thaw cycles. This method was not sophisticated in terms of efficiency of radiolabeling and prevention of occupational irradiation. Recently, Marik et al.[11] synthesized a radiolabeled amphiphilic compound for determining liposomal distribution by PET, although their method is not applicable to preformed liposomes.

In the present study, we developed not only novel [^{18}F]-positron-labeled compounds for liposomal labeling but also a new universal methodology for rapid and one-step labeling of preformed liposomes. Potent compounds were selected from a diversity of synthesized amphiphilic compounds through a series of in vitro nonradioisotope (non-RI) and RI screening studies. On the basis of the results of these studies, the structures of [^{18}F]-labeled compounds were optimized. By use of these compounds, liposomes were [^{18}F]-labeled with high efficiency and liposomal trafficking in mice was visualized by real-time analysis using a planar positron imaging system (PPIS).

To conduct the experiments for a preliminary screening of liposome-labeling compounds (vide infra), we designed novel amphiphilic compounds (**2aA**−**2cE**) and prepared them as follows: Sharma's Yb(OTf)$_3$-catalyzed etherification method[12] was applied to the coupling of the known benzyl alcohol **1a**[13] having a lipophilic *n*-octyl group to commercial diethylene glycol. The reaction proceeded gradually at 50 °C to afford **2aA**. Commercial poly(ethylene glycol)s (PEGs) with average molecular weights of 200, 285–315, 380–420, and 850–950 were used for preparation of **2aB**, **2aC**, **2aD**, and **2aE**, respectively. In these cases, the reactions proceeded at ambient temperature. Whereas **2aB** was obtained as a single compound having four PEG units after purification via SiO_2 chromatography, others were mixtures of several analogues having different lengths of the PEG chain, and the average number of its PEG units was indicated by "*m*". Similarly, **2bA**−**2cE** were synthesized by the reaction of **1a**,**b**[13] with diethylene glycol or the corresponding PEG.

The toluene sulfonates (**3bA**−**3bC** and **3cA**) were obtained by reactions of the sodium alkoxides derived from the corresponding **2** with TsCl.[14] Purification of crude products via SiO_2 chromatography afforded **3bA**−**3bC** and **3cA**, each as a single compound. In the same manner, the toluene sulfonates (**6a** and **6b**) without the aromatic group were prepared from commercially available **5a**,**b**. The fluorinated compounds (**4bA**−**4bC**, **4cA**, **7a**, and **7b**) were prepared as references for the [^{18}F]-labeled compounds ([^{18}F]**4** and [^{18}F]**7**) by the direct fluorination of the corresponding alcohols (**2** and **5**) with (diethylamino)sulfur trifluoride (DAST, Scheme 1).[15] The preparation of the [^{18}F]-labeled compounds ([^{18}F]**4bA**−**4bC**, [^{18}F]**4cA**, [^{18}F]**7a**, and [^{18}F]**7b**) was effectively achieved via nucleophilic substitution of the corresponding toluene sulfonates (**3** and **6**) with [^{18}F]KF/K[2.2.2] obtained by the previously reported method[16] with minor modifications (Scheme 2).

* To whom correspondence should be addressed. Phone: +81-54-264-5701. Fax: +81-54-264-5705. E-mail: oku@u-shizuoka-ken.ac.jp.

† Department of Medical Biochemistry and Global COE, University of Shizuoka.

‡ Department of Synthetic Organic Chemistry, University of Shizuoka.

§ Hamamatsu Photonics K.K.

[a] Abbreviations: PET, positron emission tomography; DDS, drug delivery systems; FDG, 2-deoxy-2-fluoroglucose; RI, radioisotope; PEG, poly(ethylene glycol); DAST, (diethylamino)sulfur trifluoride; HPLC, high-performance liquid chromatography; FBS, fetal bovine serum; HDL, high-density lipoprotein; DMSO, dimethyl sulfoxide; PBS, phosphate buffered saline; PPIS, planar positron imaging system.

10.1021/jm7010518 CCC: $37.00
Published on Web 12/01/2007

Scheme 1[a]

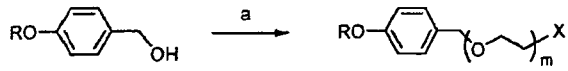

1a $R^1 = n\text{-}C_8H_{17}$
1b $R^1 = n\text{-}C_{12}H_{25}$
1c $R^1 = n\text{-}C_{16}H_{33}$

2 X = OH
3 X = OTs
4 X = F
b
c

2aA R = $n\text{-}C_8H_{17}$, m = 2, X = OH
2aB R = $n\text{-}C_8H_{17}$, m = 4, X = OH
2aC R = $n\text{-}C_8H_{17}$, m = 7, X = OH
2aD R = $n\text{-}C_8H_{17}$, m = 9, X = OH
2aE R = $n\text{-}C_8H_{17}$, m = 20, X = OH
2bA R = $n\text{-}C_{12}H_{25}$, m = 2, X = OH
2bB R = $n\text{-}C_{12}H_{25}$, m = 4, X = OH
2bC R = $n\text{-}C_{12}H_{25}$, m = 7, X = OH
2bD R = $n\text{-}C_{12}H_{25}$, m = 9, X = OH
2bE R = $n\text{-}C_{12}H_{25}$, m = 20, X = OH
2cA R = $n\text{-}C_{16}H_{33}$, m = 2, X = OH
2cB R = $n\text{-}C_{16}H_{33}$, m = 4, X = OH
2cC R = $n\text{-}C_{16}H_{33}$, m = 7, X = OH
2cD R = $n\text{-}C_{16}H_{33}$, m = 9, X = OH
2cE R = $n\text{-}C_{16}H_{33}$, m = 20, X = OH

3bA R = $n\text{-}C_{12}H_{25}$, m = 2, X = OTs
3bB R = $n\text{-}C_{12}H_{25}$, m = 4, X = OTs
3bC R = $n\text{-}C_{12}H_{25}$, m = 7, X = OTs
3cA R = $n\text{-}C_{16}H_{33}$, m = 2, X = OTs
4bA R = $n\text{-}C_{12}H_{25}$, m = 2, X = F
4bB R = $n\text{-}C_{12}H_{25}$, m = 4, X = F
4bC R = $n\text{-}C_{12}H_{25}$, m = 7, X = F
4cA R = $n\text{-}C_{16}H_{33}$, m = 2, X = F

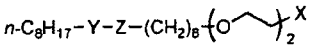

5a Y–Z = CH_2CH_2, X = OH
6a Y–Z = CH_2CH_2, X = OTs
7a Y–Z = CH_2CH_2, X = F
5b Y–Z = (*Z*)-CH=CH, X = OH
6b Y–Z = (*Z*)-CH=CH, X = OTs
7b Y–Z = (*Z*)-CH=CH, X = F
b
c

[a] Reagents and conditions: (a) $H(OCH_2CH_2)_mOH$, $Yb(OTf)_3$, $ClCH_2CH_2Cl$, 50 °C (for **2A**), room temp (for **2B–E**), 10–50% yields; (b) NaH, THF, 0 °C to room temp, then TsCl, room temp, 40–70% yields; (c) DAST, CH_2Cl_2, 0 °C to room temp, 10–35% yields.

Scheme 2[a]

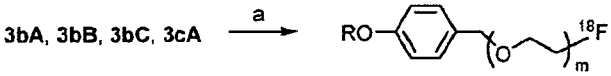

[^{18}F]**4bA** R = $n\text{-}C_{12}H_{25}$, m = 2
[^{18}F]**4bB** R = $n\text{-}C_{12}H_{25}$, m = 4
[^{18}F]**4bC** R = $n\text{-}C_{12}H_{25}$, m = 7
[^{18}F]**4cA** R = $n\text{-}C_{16}H_{33}$, m = 2

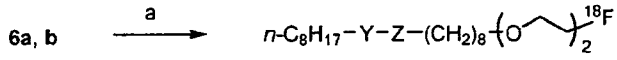

[^{18}F]**7a** Y–Z = CH_2CH_2
[^{18}F]**7b** Y–Z = (*Z*)-CH=CH

[a] Reagents and conditions: (a) [^{18}F]KF/K[2,2,2], MeCN, reflux, 10 min.

In this study, we developed a new method of liposomal labeling named the "solid-phase transition method" and determined the incorporation efficiency of the diverse nonradiolabeled compounds (**2aA−2cE**). At first, the amphiphilic compounds (**2aA−2cE**) were dried to make a thin film. Liposomes were added to the solvent-free compound (100:1 as the molar ratio of lipids to compounds) and incubated at 65 °C for 15 min. Then the liposomal solutions were transferred to centrifuge tubes, and the compounds not incorporated were removed by an ultracentrifugation. Compounds in the liposomal fraction (pellet), supernatant, and residue were quantified by HPLC. Figure 1 shows the incorporation efficiency of the various compounds. In the case of some compounds such as **2aD** and **2aE** with a shorter aliphatic hydrocarbon chain and a longer PEG chain, the incorporation efficiency was decreased. The

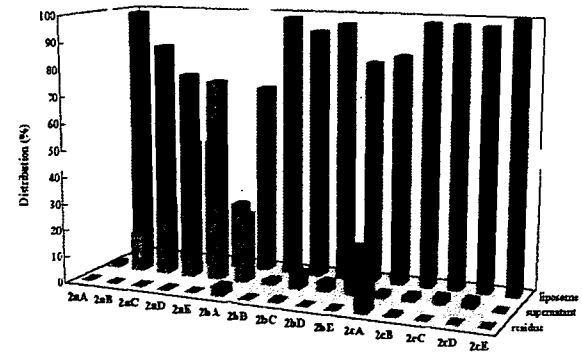

Figure 1. Efficiency of incorporation of novel amphiphilic compounds into liposomes. Incorporation experiments were performed by the solid-phase transition method, and the amount of compound in each fraction (liposome, supernatant, and residue) was determined by HPLC.

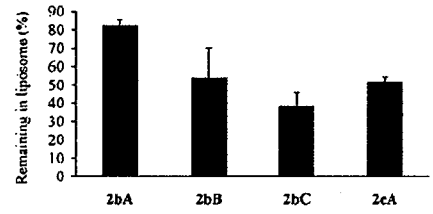

Figure 2. Stability of modified liposomes. Liposomes modified with nonradiolabeled amphiphilic compounds were incubated for 1 h in the presence of FBS, and the amounts of compounds in the liposome were determined. Data represent the mean ± standard deviation ($n = 4$).

analysis of particle size in water (data not shown) led us to consider that these compounds had formed micelles.

On the basis of the above-mentioned experiments, we selected four compounds (**2bA–2bC**, and **2cA**) that had relatively high incorporation efficiency and different physicochemical properties and examined the stability of incorporation of these compounds in the presence of serum. Liposomes were incubated at 37 °C for 1 h in the presence of 50% fetal bovine serum (FBS). It is well-known that amphiphilic compounds associated with the lipid bilayer of liposomes via weak hydrophobic interactions are transferred from liposome to serum, and that phenomenon is due mainly to high-density lipoprotein (HDL) in the serum. Liposomes and other components including serum lipoproteins were fractionated by gel filtration chromatography, and the amount of compounds that remained in the liposomal fraction was determined. Strikingly, there were significant differences among the compounds in terms of stability in serum (Figure 2), and a structure–activity relationship was indicated.

Next, the practically useful compounds 1-[^{18}F]fluoro-3,6-dioxatetracosane ([^{18}F]**7a**) and (*Z*)-1-[^{18}F]fluoro-3,6-dioxatetracos-15-ene ([^{18}F]**7b**) were prepared, and the efficiency of liposomal labeling using these [^{18}F]-labeled compounds was determined. Since the [^{18}F]-labeled compounds possessed very high radioactivity, only a very small amount of compound was needed for liposomal labeling in comparison with the amount of nonradiolabeled compounds used in the non-RI experiment mentioned above. Therefore, it is possible to conclude a difference in labeling efficiency between a trace amount of radiolabeled compounds and UV detectable non-RI compounds by use of the "solid-phase transition method". Figure 3 indicates the labeling efficiency of [^{18}F]-labeled compounds (**4bA−4bC**, **4cA**, **7a**, and **7b**). There was no significant difference between it and that of the corresponding nonradiolabeled compounds.

We then examined the stability of [^{18}F]-labeled compounds. Figure 4 indicates that there was no significant difference in

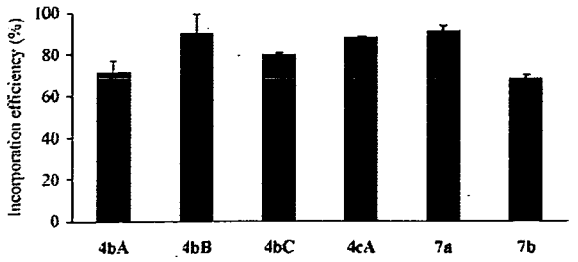

Figure 3. Incorporation efficiency of [^{18}F]-radiolabeled amphiphilic compound. Incorporation experiment with [^{18}F]-radiolabeled probe was performed by the solid-phase transition method. The incorporation efficiency was determined by measuring γ-ray radioactivity. The data represent the mean ± standard deviation (n = 4).

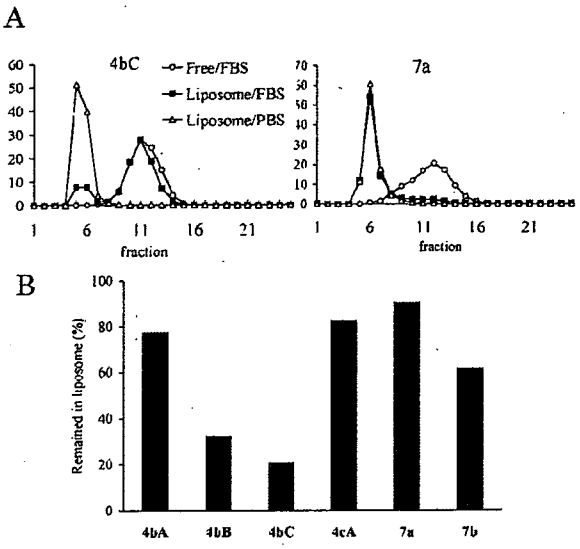

Figure 4. Stability in the serum of liposomes modified with [^{18}F]-radiolabeled amphiphilic compounds. Liposomes modified with [^{18}F]-radiolabeled amphiphilic compounds were incubated in the presence or absence of FBS for 30 min. The reactants were fractionated by gel filtration chromatography, and the radioactivity of each fraction was measured. (A) Typical elution patterns are shown: liposome fractions 5–9; serum lipoprotein fractions 9–16. (B) The radioactivity in liposome fractions is shown.

stability in liposomes between non-RI and RI compounds. These results proved the feasibility of screening with nonradiolabeled compounds to obtain appropriate radiolabeled compounds. Interestingly enough, although there is only one difference in the structures between [^{18}F]**7a** and [^{18}F]**7b**, which is the presence of an unsaturated bond in the aliphatic hydrocarbon chain of the latter, the stability of [^{18}F]**7a** in serum was much better. Therefore, we selected [^{18}F]**7a** as the probe with the most potential for in vivo imaging of liposomes.

It is well-known that one of the most important elements in trafficking of liposomes in vivo is the diameter of the particles. Larger-sized liposomes are quickly trapped by the reticuloendothelial system (RES) in the liver and spleen. To demonstrate the usefulness of [^{18}F]**7a**, we examined the typical in vivo behavior of differently sized liposomes. We prepared ^{18}F-labeled liposomes with three different diameters, namely, 90, 170, and 570 nm, as well as the liposome-free compound dispersed in 1% DMSO/PBS, and injected them into mice via a tail vein. Whole-body imaging of [^{18}F]**7a** in normal mice was obtained by using PPIS. Real-time imaging from PPIS showed that the larger the liposomes, the more the liposomes were trapped and accumulated in the spleen (Figure 5A). These imaging results

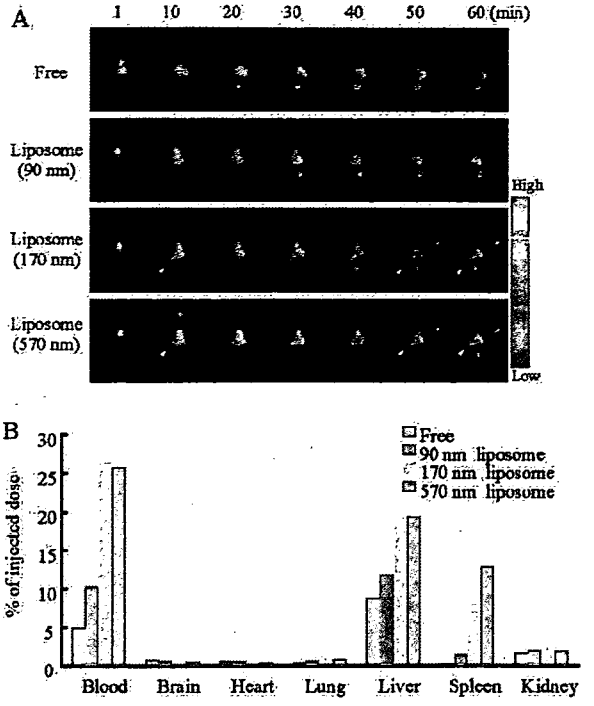

Figure 5. Whole-body imaging of [^{18}F]**7a** and liposome labeled with [^{18}F]**7a** in BALB/c mice by use of PPIS. Each radiolabeled sample at a dose of 2.5 MBq was injected via a tail vein. (A) Data were acquired with a 1 min frame at 1, 10, 20, 30, 40, 50, and 60 min after injection. Liposomes with diameters of 170 and 570 nm were accumulated in spleen (white arrowheads) and liver (green arrowheads). (B) Shown is the biodistribution in BALB/c mice after intravenous injection of [^{18}F]**7a** or liposomes labeled with [^{18}F]**7a**.

were also supported by the data from radioactivity at autopsy (Figure 5B). In contrast, the free compound accumulated in the kidneys immediately after injection and was then excreted in the urine. This result reflected the nature of liposomes. These results suggest that this novel methodology of noninvasive real-time whole-body imaging enables us to visualize the behavior of various kinds of liposomes or lipidic particles such as lipid complexes and lipid microspheres. Also, this technique may be applied to larger animal models and three-dimensional imaging provided by PET. In the future, it may be possible to use this technique for the detection of liposomal behavior in preclinical and clinical studies. Moreover, when lipidic particles specifically targeted to disease sites are developed, these particles will be useful not only for drug delivery but also for diagnostic imaging of the sites by use of the present technology.

In summary, here we introduced novel [^{18}F]-labeled amphiphilic compounds for liposomal modification that were highly incorporated into liposomes and stable in serum. This universal method of liposomal modification, i.e., the solid-phase transition method, can be used for various kinds of liposomes and lipidic particles. The compounds are useful as PET probes for imaging liposomal trafficking in the living body. An in vivo study with PPIS revealed the feasibility of the developed ^{18}F-probe. These findings suggest that [^{18}F]**7a** is a promising PET probe for imaging of liposomal behavior. Furthermore, only one or a few kinds of ^{18}F-probe can be applied to various kinds of liposomes and lipidic particles. Further study should clarify the usefulness and utility of the current probes and methodology in preclinical and clinical studies on lipidic particle-based DDS drugs.

Acknowledgment. We acknowledge the technical assistance of Dr. T. Kakiuchi in the in vivo study (Hamamatsu Photonics K.K.) and the chemical synthesis conducted by T. Baba, N. Fujiwara, M. Hyodo, Y. Kawanishi, Y. Morikawa, H. Nemoto, T. Sato, and Y. Terauchi (Department of Synthetic Organic Chemistry, University of Shizuoka). This study was supported by a grant from Central Shizuoka Cooperation of Innovative Technology and Advanced Research in Evolution Area (City Area) supported by the Ministry of Education, Culture, Sports, Science, and Technology, Japan.

Supporting Information Available: Experimental procedures and characterization data for all new compounds; details of incorporation experiments, in vitro stability assays using non-RI and RI compounds, and mice positron imaging studies. This material is available free of charge via the Internet at http://pubs.acs.org.

References

(1) Minko, T.; Pakunlu, R. I.; Wang, Y.; Khandare, J. J.; Saad, M. New generation of liposomal drugs for cancer. *Anticancer Agents Med. Chem.* **2006**, *6*, 537–552.

(2) Pedroso de Lima, M. C.; Neves, S.; Filipe, A.; Duzgunes, N.; Simoes, S. Cationic liposomes for gene delivery: from biophysics to biological applications. *Curr. Med. Chem.* **2003**, *10*, 1221–1231.

(3) Adler-Moore, J. AmBisome targeting to fungal infections. *Bone Marrow Transplant.* **1994**, *14* (Suppl. 5), S3–S7.

(4) Kramer, M.; Miller, J. W.; Michaud, N.; Moulton, R. S.; Hasan, T.; Flotte, T. J.; Gragoudas, E. S. Liposomal benzoporphyrin derivative verteporfin photodynamic therapy. Selective treatment of choroidal neovascularization in monkeys. *Ophthalmology* **1996**, *103*, 427–438.

(5) Tomii, Y. Lipid formulation as a drug carrier for drug delivery. *Curr. Pharm. Des.* **2002**, *8*, 467–474.

(6) Buchan, P. Smarter candidate selection—utilizing microdosing in exploratory clinical studies. *Ernst Schering Res. Found. Workshop* **2007**, *59*, 7–27.

(7) Bergstrom, M.; Grahnen, A.; Langstrom, B. Positron emission tomography microdosing: a new concept with application in tracer and early clinical drug development. *Eur. J. Clin. Pharmacol.* **2003**, *59*, 357–366.

(8) Wang, J.; Maurer, L. Positron emission tomography: applications in drug discovery and drug development. *Curr. Top. Med. Chem.* **2005**, *5*, 1053–1075.

(9) Oku, N.; Tokudome, Y.; Tsukada, H.; Kosugi, T.; Namba, Y.; Okada, S. In vivo trafficking of long-circulating liposomes in tumour-bearing mice determined by positron emission tomography. *Biopharm. Drug Dispos.* **1996**, *17*, 435–441.

(10) Oku, N.; Tokudome, Y.; Tsukada, H.; Okada, S. Real-time analysis of liposomal trafficking in tumor-bearing mice by use of positron emission tomography. *Biochim. Biophys. Acta* **1995**, *1238*, 86–90.

(11) Marik, J.; Tartis, M. S.; Zhang, H.; Fung, J. Y.; Kheirolomoom, A.; Sutcliffe, J. L.; Ferrara, K. W. Long-circulating liposomes radiolabeled with [^{18}F]fluorodipalmitin ([^{18}F]FDP). *Nucl. Med. Biol.* **2007**, *34*, 165–171.

(12) Sharma, G. V. M.; Mahalingam, A. K. A facile conversion of alcohols into *p*-methoxybenzyl ethers (PMB-ethers) using *p*-methoxybenzyl alcohol-Yb(OTf)$_3$. *J. Org. Chem.* **1999**, *64*, 8943–8944.

(13) Percec, V.; Dulcey, A. E.; Balagurusamy, V. S. K.; Miura, Y.; Smidrkal, J.; Peterca, M.; Nummelin, S.; Edlund, U.; Hudson, S. D.; Heiney, P. A.; Duan, H.; Magonov, S. N.; Vinogradov, S. A. Self-assembly of amphiphilic dendritic dipeptides into helical pores. *Nature* **2004**, *430*, 764–768.

(14) The reactions of **2** and *p*-TsCl in the presence of an excess amount of pyridine resulted in complete cleavage of the benzylic ether linkage.

(15) The condition of each reaction was not optimized.

(16) Harada, N.; Ohba, H.; Fukumoto, D.; Kakiuchi, T.; Tsukada, H. Potential of [^{18}F]β-CFT-FE (2β-carbomethoxy-3β-(4-fluorophenyl)-8-(2-[^{18}F]fluoroethyl)nortropane) as a dopamine transporter ligand: a PET study in the conscious monkey brain. *Synapse* **2004**, *54*, 37–45.

JM7010518

THE JOURNAL OF BIOLOGICAL CHEMISTRY VOL. 282, NO. 11, pp. 8276–8283, March 16, 2007

Junctional Adhesion Molecule-C Promotes Metastatic Potential of HT1080 Human Fibrosarcoma*

Received for publication, September 13, 2006, and in revised form, November 29, 2006 Published, JBC Papers in Press, January 16, 2007, DOI 10.1074/jbc.M608836200

Chiaki Fuse, Yuuki Ishida, Tomoya Hikita, Tomohiro Asai, and Naoto Oku[1]

From the Department of Medical Biochemistry and Center of Excellence Program in the 21st Century, School of Pharmaceutical Sciences, University of Shizuoka, Shizuoka 422-8526, Japan

The junctional adhesion molecule (JAM) family is a key molecule in a process called transendothelial migration or diapedesis. Here, we report implications of JAM-C in cancer metastasis. We first determined the mRNA expression of JAMs in 19 kinds of cancer cell lines. JAM-C was expressed in most of tumors having potent metastatic properties. Especially in murine K-1735 melanoma cell lines, the highly metastatic sublines (M2 and X21) strongly expressed JAM-C when compared with the poorly metastatic ones (C-10 and C23). Next, we investigated the role of JAM-C in cancer metastasis by using human JAM-C (hJAM-C) gene-transfected HT1080 fibrosarcoma cells. In comparison with mock-transfected HT1080 cells, these cells showed a significant increase in the adhesion to various extracellular substrates and the invasion across a Matrigel™-coated membrane. The knockdown of hJAM-C using small interfering RNA resulted in the suppression of both the adhesion and the invasion of HT1080 cells, suggesting that endogenous hJAM-C might be involved in tumor metastasis. Finally, we studied the role of hJAM-C in an *in vivo* experimental metastatic model. The results showed that the overexpression of hJAM-C in HT1080 cells significantly decreased the life spans of the tumor-bearing mice. In contrast, the knockdown of hJAM-C in HT1080 cells suppressed the weight gain of the lungs with metastatic colonies. We conclude that the expression of JAM-C promotes metastasis by enhancing both the adhesion of cancer cells to extracellular matrices and the subsequent invasion.

Cancer metastasis involves a series of events that include dissociation of malignant cells from a primary site, polarized proteolysis and migration, intravasation into the circulatory system, and adhesion to the vascular endothelium followed by extravasation, invasion, and growth at distant sites (1). Certain cell surface molecules are known to be involved in these processes. For instance, integrins play central roles in regulating cell adhesion, motility, invasion, and angiogenesis (2–4), and matrix metalloproteinases on tumor cells can degrade the extracellular matrix (ECM)[2] (5). In particular, cell adhesion molecules play key roles in tumor adhesion and invasion, resulting in metastasis (6). When compared with normal tissues, malignant tumors are characterized by disrupted tissue architecture and deranged differentiation. Changes in the expression or function of cell adhesion molecules contribute to tumor progression both by altering the adhesion status of the cell and by affecting cell signaling (7). It has been reported that alteration of cell-cell and/or cell-matrix interactions accounts for the ability of cancerous cells to cross tissue boundaries and to disseminate to distant sites. Many adhesion molecules implicated in tumor metastasis have been identified (6), and certain of them belong to the immunoglobulin superfamily (8). Recently, the junctional adhesion molecule (JAM) family, a member of the immunoglobulin superfamily, has become a focus of study in relation to cell-cell and/or cell-matrix interactions.

The JAM family, belonging to the larger cortical thymocyte *Xenopus* molecular family (9), is a glycoprotein. It has two immunoglobulin folds (V_H and C2 type) and two extra cysteine residues in its extracellular region, a potential *N*-glycosylation site (s), and a PDZ protein-interacting domain in its intracellular region (10). JAM molecules are selectively expressed in a variety of human organs (11–13). In particular, JAMs are strongly expressed in close proximity to tight junction strands of polarized endothelial and epithelial cells and on circulating leukocytes and platelets (14, 15).

JAMs are known to not only form homophilic binding but also to interact with certain ligands in a heterophilic manner (16–20). It has been reported that JAM-A binds to $\beta 2$ integrin LFA-1 (21), that JAM-B interacts with $\alpha 4\beta 1$ integrin (22), and that JAM-C is a counter-receptor for the leukocyte integrin Mac-1 (15). Several cytoplasmic partners associated with the PDZ domain of the JAMs have also been reported (23–28). These interactions represent the likely determinants for the diverse roles of JAMs such as junction assembly, platelet activation, and leukocyte transmigration (10). In inflammation, the JAMs play an important role on the passage of leukocytes across interendothelial spaces (29, 30). Certain adhesion molecules on leukocytes and endothelial cells are known to control sequential steps in leukocyte migration (31). The steps of leukocyte migration are partly similar to those of cancer metastasis in several respects; *e.g.* both leukocytes and tumor cells need to adhere to the vascular bed and to cross the border of endothelial cells.

*The costs of publication of this article were defrayed in part by the payment of page charges. This article must therefore be hereby marked "*advertisement*" in accordance with 18 U.S.C. Section 1734 solely to indicate this fact.

[1] To whom correspondence should be addressed: Dept. of Medical Biochemistry, School of Pharmaceutical Sciences, University of Shizuoka, 52-1 Yada, Suruga, Shizuoka 422-8526, Japan. Tel.: 81-54-264-5701; Fax: 81-54-264-5705; E-mail: oku@u-shizuoka-ken.ac.jp.

[2] The abbreviations used are: ECM, extracellular matrix; JAM, junctional adhesion molecule; FBS, fetal bovine serum; PBS, phosphate-buffered saline; GFP, green fluorescent protein; EGFP, enhanced GFP; siRNA, small interfering RNA; Mock, mock-transfected.

In the present study, we investigated certain aspects of the participation of JAMs in cancer metastasis. At first, we determined the expression of JAMs in 14 cell lines and also in five sublines of the K-1735 murine melanoma. Next, we focused on the function of JAM-C in cancer metastasis and used HT1080 human fibrosarcoma cells (HT1080 cells) for metastatic studies. HT1080 cells transfected with human JAM-C (hJAM-C) were used in the experiment of cell adhesion, invasion, and *in vivo* metastasis for evaluating the functions of hJAM-C. The roles of endogenous hJAM-C were determined by examining the properties of HT1080 cells transfected with small interfering RNA for hJAM-C. This study provides the first evidence that hJAM-C promotes cancer metastasis.

EXPERIMENTAL PROCEDURES

Cell Culture—Murine melanoma K-1735 cell lines were established by I. J. Fidler (The University of Texas M.D. Anderson Cancer Center, Houston, TX) and kindly provided by Dr. J. Yokota (National Cancer Center Research Institute, Tokyo, Japan). Human HT1080 fibrosarcoma, C8161 melanoma, AZ-P7a gastric carcinoma, Colo205 colorectal adenocarcinoma, SUIT-2 pancreatic carcinoma, K562 erythroleukemia, murine B16BL6 melanoma, and Colon26 NL-17 carcinoma cells were maintained in RPMI 1640 medium containing 10% fetal bovine serum (FBS; Sigma-Aldrich), 100 units/ml penicillin (MP Biomedicals, Inc., Irvine, CA), and 100 μg/ml streptomycin (MP Biomedicals). Human JAM-C-transfected HT1080 cells were grown in the same medium supplemented with 400 μg/ml hygromycin B (Wako Pure Chemical Industries, Ltd. Osaka, Japan). Human A431 epidermoid carcinoma, HT-29 colon adenocarcinoma, HeLaS3 cervical cancer, Caco-2 colon carcinoma, murine Lewis lung carcinoma, and K-1735 cells were maintained in Dulbecco's modified Eagle's medium containing 10% FBS, 100 units/ml penicillin, and 100 μg/ml streptomycin. Chinese hamster ovary (CHO)-K1 cells were maintained in Ham's F12 medium containing 10% FBS and the same antibiotics. All cells were cultured at 37 °C in a humidified incubator with 5% CO_2.

Reverse Transcription and PCR—Total RNA was isolated by using TRIzol® LS reagent (Invitrogen), and cDNAs were generated from total RNA samples (5 μg) by using the SuperScript first-strand synthesis system (Invitrogen). The PCR conditions were as follows: 94 °C for 2 min; 30 cycles of 94 °C for 30 s, 50 °C for 30 s, 72 °C for 1 min; and 72 °C for 10 min. The primers for human JAM-A were 5′-CGC GAT GGG GAC AAA GGC GC-3′ (sense) and 5′-ACC AGG AAT GAC GAG GTC-3′ (antisense); for human JAM-B, 5′-TAA AAA TCG AGC TGA GAT GAT AG-3′ (sense) and 5′-TTA AAT TAT AAA GGA TTT TGT G-3′ (antisense); for human JAM-C, 5′-ACT TCT TCC TGC TGC TGC TT-3′ (sense) and 5′-TCT GAA GTC GCC CTC CTC GT-3′ (antisense); for mouse JAM-A, 5′-ATG GGC ACC GAG GGG AAA GC-3′ (sense) and 5′-TCA CAC CAG GAA CGA CGA GG-3′ (antisense); for mouse JAM-B, 5′-ATG GCG CTG AGC CGG CGG CT-3′ (sense) and 5′-TCA GAT AAC AAA GGA CGA TT-3′ (antisense); for mouse JAM-C, 5′-ATG GCG AGG AGC CCC CAA GG-3′ (sense) and 5′-TTA AAT TAT AAA GGA TTT TG-3′ (antisense); and for β-actin, 5′-TGA CGG GGT CAC CCA CAC TGT GCC CAT CTA-3′ (sense) and 5′-CTA GAA GCA TTT GCG GTG GAC GAT GGA GGG-3′ (antisense). The PCR products were applied onto 1.5% agarose gels and visualized by staining with ethidium bromide under UV light.

Western Blotting—Anti-JAM-C antibody (goat polyclonal IgG) was purchased from R&D Systems Inc. (Minneapolis, MN). Peroxidase-conjugated secondary antibody was from Santa Cruz Biotechnology Inc. (Santa Cruz, CA).

The cells on culture plates were rinsed with phosphate-buffered saline (pH 7.4, PBS). Cell extracts were prepared with lysis buffer composed of 10 mM Tris (pH 7.5), 0.1% SDS, 50 μg/ml aprotinin, 200 μM leupeptin, 2 mM phenylmethylsulfonyl fluoride, and 100 μM pepstatin A. Total protein concentration was measured by using a BCA protein assay reagent kit (Pierce) with bovine serum albumin as a standard, according to the manufacturer's instructions. The cell extracts were subjected to 10 or 15% SDS-PAGE and transferred electrophoretically to polyvinylidene difluoride membranes (Millipore, Billerica, MA). After blocking for 1 h at room temperature with 5% skim milk in Tris-HCl buffered saline containing 0.1% Tween 20 (TTBS, pH 7.4), the membranes were incubated with 0.1 μg/ml antibody for 2 h at room temperature. Then, they were incubated with peroxidase-conjugated secondary antibody at a dilution of 1:2000 to 1:10,000 for 1 h at room temperature. Each sample was developed by using chemiluminescent substrate (ECL; Amersham Biosciences).

cDNA Cloning—The hJAM-C sequence was obtained from GenBank™ (accession number AF448478). Total RNA was isolated from human umbilical vein endothelial cells (BioWhittaker, Walkersville, MD) by using TRIzol LS reagent and reverse-transcribed into single-stranded cDNA by using the SuperScript first-strand synthesis system (Invitrogen). The full-length cDNA of hJAM-C was PCR-amplified by using Ex Taq™ (TaKaRa BIO Inc., Shiga, Japan) with specific primers based on the hJAM-C nucleotide sequence that included BamHI and HindIII restriction sites: 5′-ACG TAA GCT TAT GGC GCT GAG GCG GCC ACC-3′ (sense) and 5′-ACG TGG ATC CTC AGA TCA CAA ACG ATG ACT-3′ (antisense). The PCR product was purified by use of a High Pure PCR product purification kit (Roche Diagnostics, Basel, Switzerland). Restriction enzyme digestions of PCR product and pcDNA3.1/Hygro vector (Invitrogen) were carried out at 37 °C for 1 h. Both digestion products were purified with the purification kit and then ligated at 16 °C for 2 h with T4 DNA ligase (DNA ligation kit, Version 1, TaKaRa). Competent *Escherichia coli* JM109 cells (TaKaRa) were transformed with ligation mixture, plated on Luria-Bertani (LB) agar plates, and grown overnight at 37 °C. Colonies were screened for the insert by restriction enzyme digestion, and DNA sequencing was performed at Macrogen Inc. (Seoul, Korea).

Transfection with hJAM-C—Stable GFP transfectant of HT1080 fibrosarcoma was prepared as described previously (32) and used for transfection with hJAM-C. These cells were transfected with 10 μg of pcDNA3.1/Hygro vector containing either full-length hJAM-C or no insert by using Lipofectamine™ 2000 (Invitrogen). Stable transfectant (hJAM-C/HT1080 or Mock/HT1080) was selected with 400 μg/ml hygromycin B. The expression of hJAM-C was confirmed by Western blotting as described

above. For cell growth assay, hJAM-C/HT1080 or Mock/HT1080 cells (1.0×10^5 cells/dish) were cultured for 24, 48, 72, or 96 h. After staining with 0.5% trypan blue, the numbers of living cells were counted at each time point.

Localization of hJAM-C—Human JAM-C/HT1080 or Mock/HT1080 cells were fixed with 3.7% paraformaldehyde in PBS. The cells were then blocked with 3% bovine serum albumin in PBS, incubated with 0.1 μg/ml anti-JAM-C goat polyclonal antibody for 2 h, and immersed in 1.0 μg/ml Alexa Fluor® 555-labeled anti-goat IgG secondary antibody (Molecular Probes Inc., OR) for 1 h. Localization of hJAM-C was determined by using a LSM510 Meta confocal system (Carl Zeiss Co., Ltd.).

Adhesion Assay—Ninety-six-well flat-bottomed plates were dry-coated with Matrigel™ (3 μg/well), fibronectin (0.75 μg/well), vitronectin (0.25 μg/well), laminin (1.25 μg/well), or type IV collagen (1.5 μg/well) and blocked with 1% bovine serum albumin for 1 h. Human JAM-C/HT1080 or Mock/HT1080 cells (5×10^4 cells/well) were allowed to adhere to each substrate-coated well at 37 °C for 1 h. After washing with PBS, the adherent cells were stained with crystal violet for 10 min. The pigment was extracted with 33% acetic acid for 5 min, and the absorbance was measured at 570 nm as an indicator of adherent cells.

Invasion Assay—The invasion was evaluated as the capacity of hJAM-C/HT1080 cells to pass through a Matrigel-coated transwell insert. BD Matrigel matrix (25 μg/well; BD Biosciences) was coated on a fluorescence-blocking micropore membrane of a culture insert (8-μm pore size, 0.28 cm^2, Falcon HTS FluoroBlok™ inserts, BD Biosciences). The culture inserts were set into wells of a 24-transwell plate containing RPMI 1640 medium supplemented with 10% FBS, which had not been heat-immobilized, as a chemoattractant. After the cell density had been adjusted to 5×10^5 cells/ml in serum-free medium, 5×10^4 cells in 100 μl were introduced into each culture insert. After incubation for 4–5 h at 37 °C in a CO_2 incubator, the cells that traversed the Matrigel layer and attached to the lower surface of the filter were counted in five randomized fields under a fluorescence microscope.

Transfection with siRNA—The nucleotide sequences of siRNA with a two-nucleotide overhang (underline) for hJAM-C were 5′-CAGGAUGGAGAAAGUUACAAGAACCAG-3′ (sense) and 5′-GGUUCUUGUAACUUUCUCCAUCCUGAU-3′ (antisense); those for luciferase were 5′-UGGUUUACCUAAAGGUGUACGAAUUAG-3′ (sense) and 5′-AAUUCGUACACCUUUAGGUAAACCAAU-3′ (antisense); and those for EGFP were 5′-GGCUACGUCCAGGAGCGCACC-3′ (sense) and 5′-UGCGCUCCUGGACGUAGCCUU-3′ (antisense). The sequences for hJAM-C, luciferase, and EGFP correspond to nucleotide regions 829–853, 612–636, and 118–141, respectively. The siRNAs for luciferase and EGFP were used as a control siRNA. All siRNAs were prepared by Hokkaido System Science Co. (Hokkaido, Japan). Stable GFP transfectant of HT1080 fibrosarcoma (31) was transfected with siRNA by using Lipofectamine 2000 according to the manufacturer's instructions. Forty-eight hours after the addition of siRNA/Lipofectamine 2000 complexes, the knockdown of hJAM-C was evaluated by Western blotting. In all experiments using siRNA, siRNA-transfected HT1080 cells were used at 48 h after the addition of these complexes. Western blotting and cell growth, adhesion, and invasion assays were performed by methods similar to those described above.

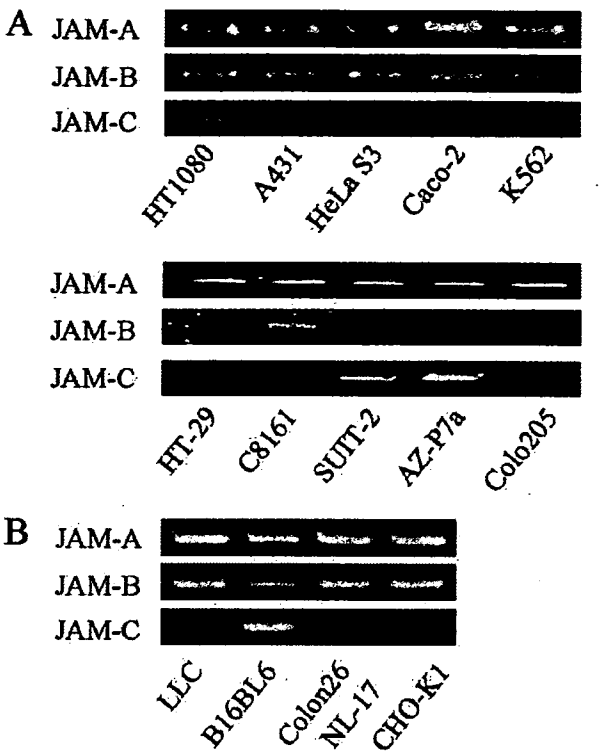

FIGURE 1. **Expression of JAM transcripts in various cancer cell lines.** Total mRNA was prepared from each cell line, and reverse transcription-PCR was performed. PCR products were visualized by ethidium bromide staining under UV light. *A*, human cell lines as follows: *HT1080*, fibrosarcoma; *A431*, epidermoid carcinoma; *HeLaS3*, cervical cancer; *Caco-2*, colon carcinoma; *K562*, erythroleukemia; *HT-29*, colon adenocarcinoma; *C8161*, melanoma; *SUIT-2*, pancreatic carcinoma; *AZ-P7a*, gastric carcinoma; *Colo205*, colon adenocarcinoma. *B*, rodent cell lines as follows: *LLC*, murine Lewis lung carcinoma; *B16BL6*, murine melanoma; *Colon26 NL-17*, murine colon carcinoma; *CHO-K1*, Chinese hamster ovarian cancer.

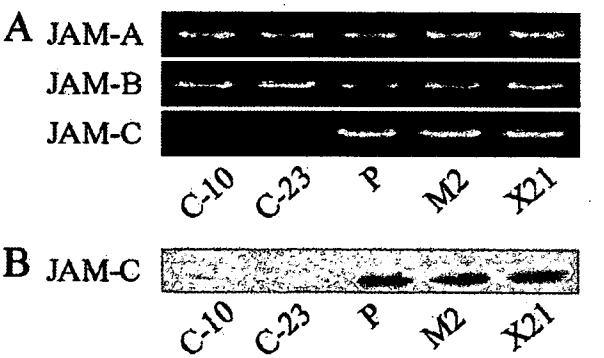

FIGURE 2. **Expression of JAMs in K-1735 murine melanoma.** *A*, reverse transcription-PCR for detection of JAM-A, JAM-B, and JAM-C transcript was performed. C-10 and C-23 are poorly metastatic sublines, whereas M2 and X21 are highly metastatic ones. *P* indicates parent K-1735 melanoma. *B*, Western blotting analysis was performed to determine the expression of JAM-C protein in each K-1735 cell line.

Experimental Metastasis—The influence of the overexpression and the knockdown of hJAM-C on tumor metastasis were evaluated in an experimental pulmonary metastatic model. Cells were harvested from culture plates by brief exposure to

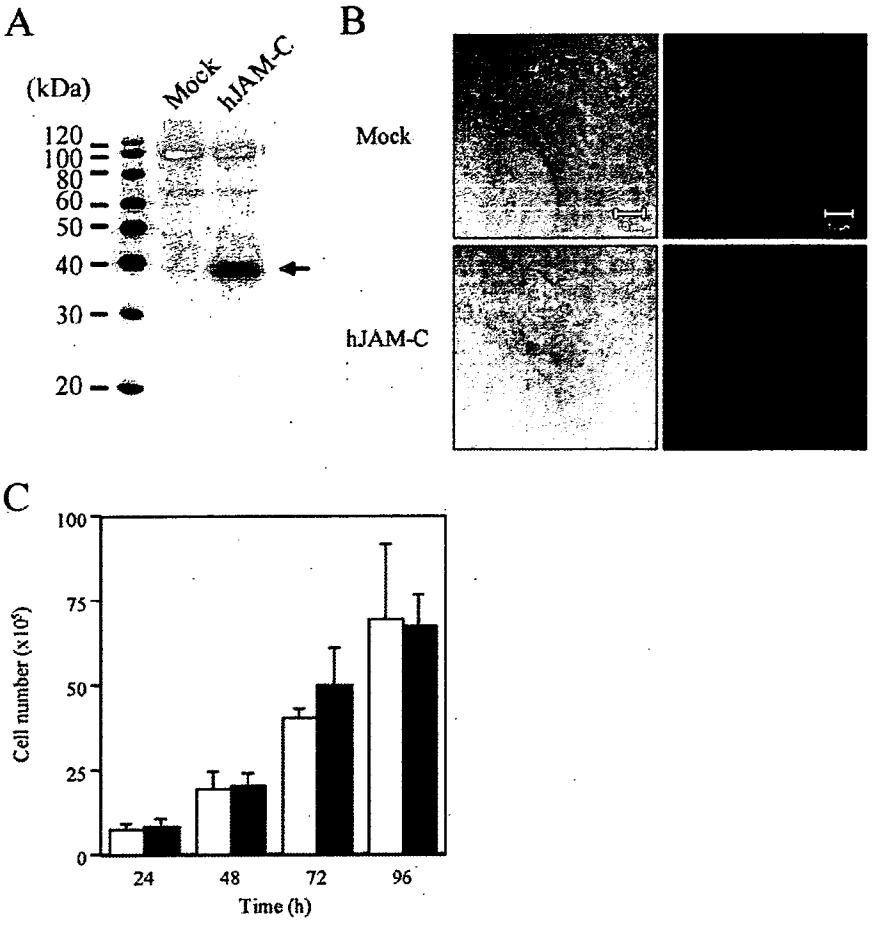

FIGURE 3. **Characterization of hJAM-C-transfected HT1080 cells.** *A*, the amount of hJAM-C in Mock/HT1080 or hJAM-C/HT1080 cells was determined by Western blotting. The *arrow* points to JAM-C. *B*, localization of hJAM-C on Mock/HT1080 or hJAM-C/HT1080 cells was visualized. The *left panels* show the morphology of these cells observed by differential interference contrast microscopy; the *right panels* show the distribution of hJAM-C (*red fluorescence*) observed by confocal laser scanning microscopy. *C*, the proliferation of Mock/HT1080 (*open bars*) and hJAM-C/HT1080 (*closed bars*) cells was determined at the indicated times. Cell number was counted at each time point. Data are the mean ± S.D. ($n = 4$).

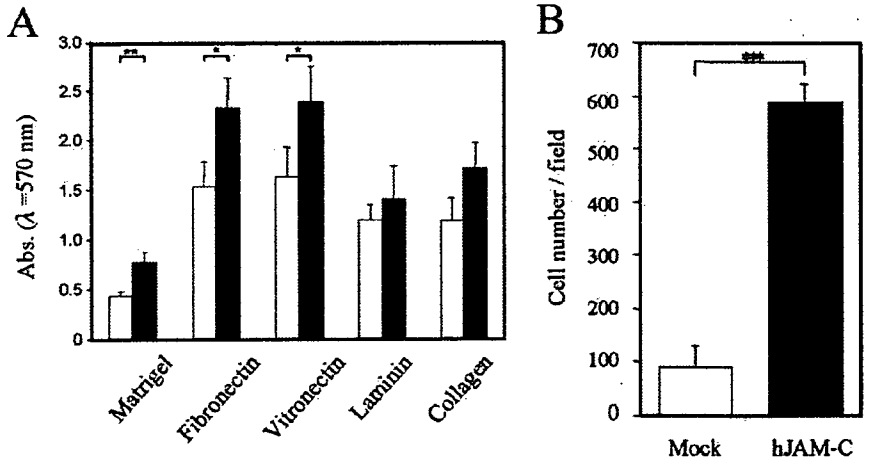

FIGURE 4. **Increased adhesion and invasion of hJAM-C/HT1080 cells.** *A*, the adherence of hJAM-C/HT1080 cells to various purified extracellular substrates was examined. Data show the mean absorbance (*Abs.*) of crystal violet taken up by the adherent cells. *Bars* indicate Mock/HT1080 cells (*open bars*) and hJAM-C/HT1080 cells (*closed bars*). *B*, an invasion assay was performed on Mock/HT1080 and hJAM-C/HT1080 cells. The number of cells that invaded through the Matrigel-coated membrane was counted under a fluorescence microscope. Significant differences between Mock/HT1080 and hJAM-C/HT1080 cells are indicated: *, $p < 0.05$; **, $p < 0.01$; ***, $p < 0.001$. *Bars* indicate ± S.D.

0.02% EDTA/PBS. After the cells had been centrifuged and resuspended in the medium, their concentration was adjusted to 5×10^6 cells/ml. For evaluating the effect of overexpression of hJAM-C on metastatic potential, hJAM-C/HT1080 or Mock/HT1080 cells (1×10^6 cells/mouse) were injected into the tail vein of 4-week-old BALB/c nu/nu male mice (Charles River Japan Inc., Kanagawa, Japan). The life spans of tumor-bearing mice were monitored ($n = 10$ for mock/HT1080, $n = 11$ for hJAM-C/HT1080). In another three mice in each group, the lungs were dissected, weighed, and photographed for evaluating metastasis at 19 days after implantation.

For evaluating the effect of knockdown of hJAM-C on metastatic potential, hJAM-C siRNA- or EGFP siRNA-treated cells (1×10^6 cells/mouse) were injected into the tail vein of 9-week-old BALB/c nu/nu male mice ($n = 4$). The lungs with tumor metastases were dissected, weighed, and photographed at 38 days after implantation.

Histochemical Analysis—The lungs with metastatic colonies were embedded in optimal cutting temperature compound (Sakura Finetechnochemical Co., Ltd., Tokyo, Japan) and frozen at −80 °C. Six-micrometer lung sections were prepared by using a cryostatic microtome (HM 505E, Microm, Walldorf, Germany), stained with hematoxylin-eosin, and examined histopathologically.

Statistical Analysis—Statistical analysis (mean value, S.D., independent *t* test) was performed by using Stat View® 4.0 (SAS Institute Inc., Cary, NC). Results were expressed as the mean ± S.D.

RESULTS

The amounts of JAM transcripts in cancer cell lines were determined by reverse transcription-PCR. In this experiment, we used 19 kinds of cancer cells lines. Among them, human HT1080 fibrosarcoma, HT-29 colon adenocarcinoma, C8161 melanoma,

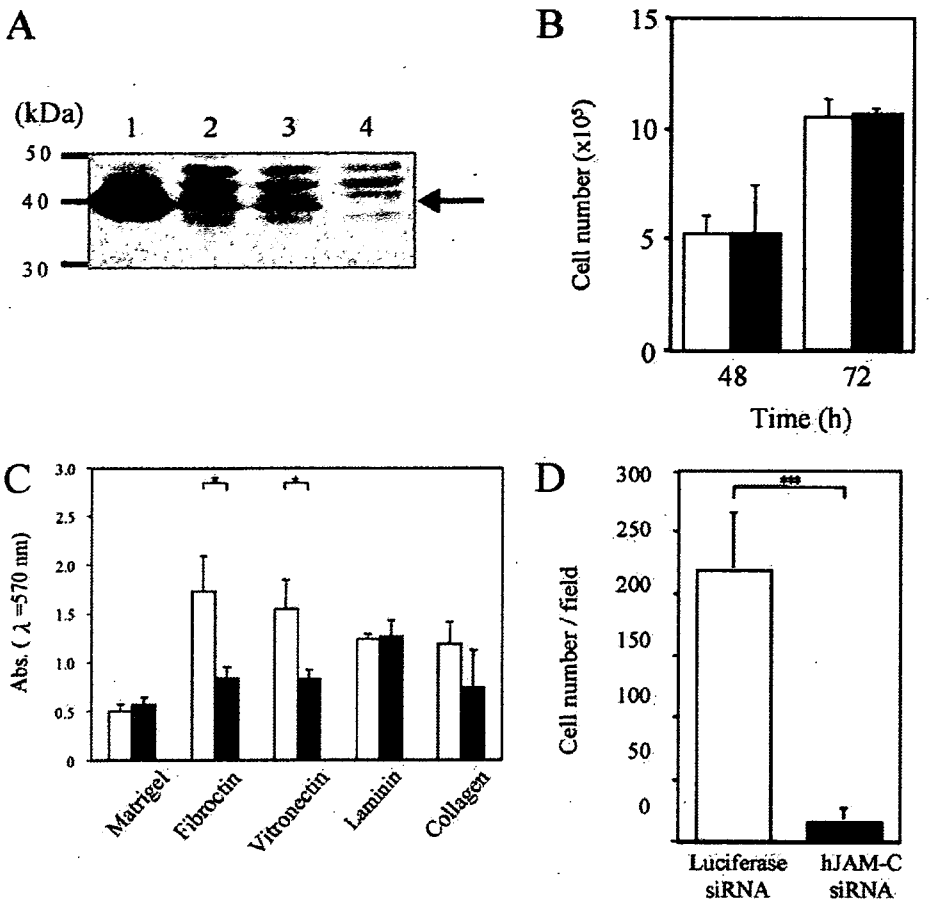

FIGURE 5. **Involvement of endogenous hJAM-C in invasion of HT1080 cells.** *A*, Western blotting analysis of hJAM-C expression in hJAM-C-overexpressing hJAM-C/HT1080 cells (*lane 1*), HT1080 cells (*lane 2*), luciferase siRNA-transfected HT1080 cells (*lane 3*), and hJAM-C siRNA-transfected HT1080 cells (*lane 4*) was performed. Luciferase siRNA-transfected and hJAM-C siRNA-transfected HT1080 cells were used for each experiment at 48 h after transfection. *B*, the proliferation of luciferase siRNA-transfected (*open bars*) and hJAM-C siRNA-transfected (*closed bars*) HT1080 cells was determined at the indicated times. Cell number was counted at each time point. Data are the mean ± S.D. ($n = 4$). *C*, adhesion of EGFP siRNA-transfected (*open bars*) and hJAM-C siRNA-transfected (*closed bars*) HT1080 cells to extracellular substrates are shown. The experimental procedures were similar to the case of the hJAM-C overexpression study. Significant differences between EGFP siRNA-transfected and hJAM-C siRNA-transfected HT1080 cells are indicated: *, $p < 0.05$. *Bars* indicate mean ± S.D. *D*, invasion assay using luciferase siRNA-transfected (*open bars*) and hJAM-C siRNA-transfected (*closed bars*) HT1080 cells was performed. The number of cells that invaded through the Matrigel-coated membrane was counted under a fluorescence microscope. Significant differences between luciferase siRNA-transfected and hJAM-C siRNA-transfected HT1080 cells are indicated: ***, $p < 0.001$. *Bars* indicate mean ± S.D.

SUIT-2 pancreatic carcinoma, AZ-P7a gastric carcinoma, and murine Lewis lung carcinoma, B16BL6 melanoma, Colon26 NL-17 carcinoma, K-1735 M2, and X21 melanoma cell lines were known to have highly metastatic characteristics. The transcripts of JAM-A were similar in amount regardless of the cancer cell lines (Fig. 1). In contrast, the expression levels of JAM-B and JAM-C were different among the various cell lines. The transcripts of JAM-C were detected in highly metastatic cell lines such as HT1080 fibrosarcoma, SUIT-2 pancreatic carcinoma, AZ-P7a gastric carcinoma, Lewis lung carcinoma, B16BL6 melanoma, and Colon26 NL-17 carcinoma (Fig. 1). To assess the relationship between the amounts of JAM transcripts in tumor cells and their metastatic potentials, the expression of JAM members was compared in K-1735 murine melanoma subpopulations having diverse biologic behavior (33). Each clone (C-10, C-23, M2, and X21) was previously established from the parent K-1735 cells. The *in vivo* metastatic potential of M2 and X21 sublines is very high, as is that of the parent K-1735 cells, whereas that of C-10 and C-23 clones is quite poor. As shown in Fig. 2*A*, the mRNA level of JAM-C was markedly up-regulated in the parent K-1735 and highly metastatic sublines (M2 and X21) when compared with that in the poorly metastatic sublines (C-10 and C-23). In contrast, the mRNA level of either JAM-A or JAM-B was not much different between the highly metastatic and poorly metastatic cells. Actual expression levels of JAM-C protein in K-1735 sublines determined by Western blotting correlated well with those of JAM-C mRNA (Fig. 2*B*).

JAM-C functions in cancer metastasis were explored by constructing hJAM-C-overexpressing HT1080 fibrosarcoma cells. HT1080 cells were transfected with hJAM-C-encoded pcDNA3.1/Hygro vector (hJAM-C/HT1080) or empty vector (Mock/HT1080). Overexpression of hJAM-C in hJAM-C/HT1080 cells was confirmed by Western blotting. As shown in Fig. 3*A*, the amount of hJAM-C protein was very abundant in hJAM-C/HT1080 cells than in Mock/HT1080 cells. Human JAM-C in the transfectant was localized on the extensions of its plasma membrane (Fig. 3*B*). The forced expression of hJAM-C did not affect the cell growth rate (Fig. 3*C*).

To evaluate the participation of hJAM-C in the interaction of the cells with ECM, the adhesion of hJAM-C/HT1080 cells to various ECM components was investigated. Human JAM-C expression in HT1080 cells significantly increased their adhesion to Matrigel, fibronectin, and vitronectin and slightly increased their adhesion to type IV collagen and laminin (Fig. 4*A*). Next, the effect of hJAM-C overexpression on tumor cell invasion was examined. The number of cells that invaded through a Matrigel-coated membrane was compared between hJAM-C/HT1080 and Mock/HT1080 cells. The migration of HT1080 cells was significantly accelerated by the overexpression of hJAM-C, suggesting that hJAM-C expression might be correlated with tumor malignancy (Fig. 4*B*).

To confirm whether endogenous JAM-C was involved in the invasion, hJAM-C siRNA-transfected HT1080 cells were prepared. The expression of endogenous hJAM-C was observed in both control and luciferase siRNA-transfected HT1080 cells to some extent, and the knockdown of endogenous hJAM-C was

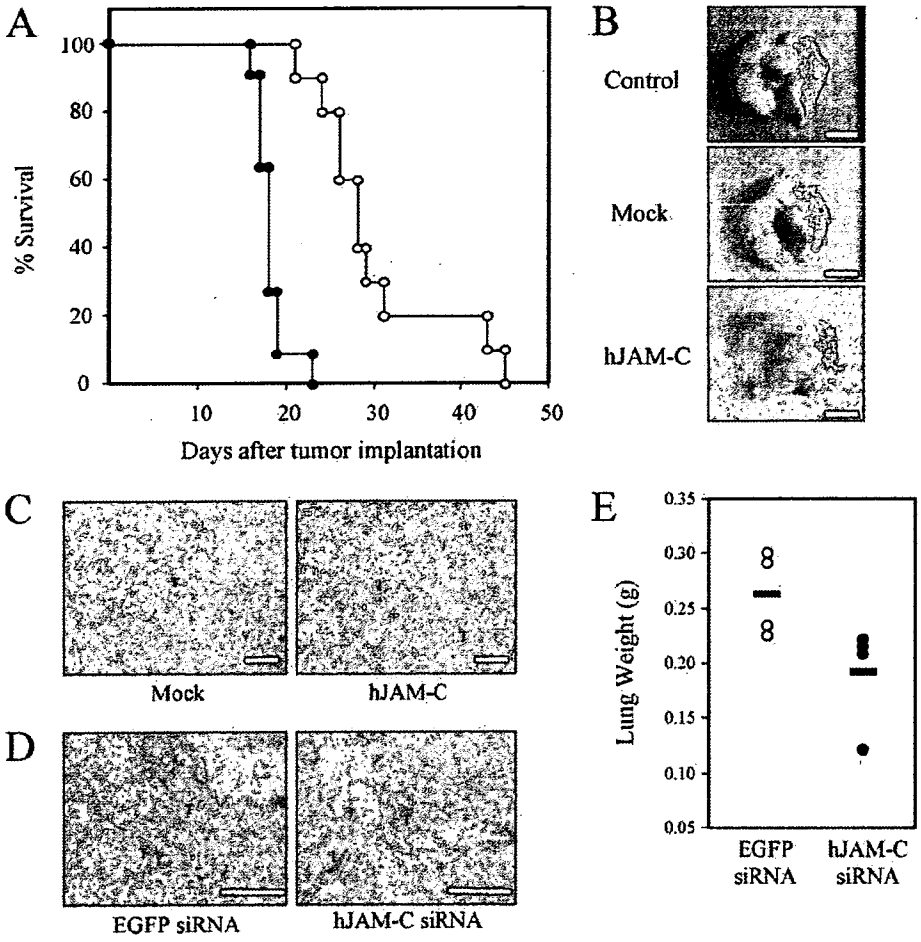

FIGURE 6. **Influences of hJAM-C expression on pulmonary metastasis of HT1080 cells.** *A*, the survival times of BALB/c nu/nu mice that had been inoculated with Mock/HT1080 ($n = 10$, *open circle*) or hJAM-C/HT1080 ($n = 11$, *closed circle*) cells were determined. After intravenous inoculation of these cells, the life spans of tumor-bearing mice were monitored. *B*, the morphology of the lungs bearing Mock/HT1080 or hJAM-C/HT1080 fibrosarcoma was examined. The lungs of each group were dissected and photographed at 19 days after inoculation. *Scale bars* represent 5 mm. *C*, histochemical analysis of the lung with metastatic colonies was performed in the hJAM-C overexpression experiment. At 19 days after inoculation, the lung sections were prepared and stained with hematoxylin-eosin. *Scale bars* represent 500 μm. *T* indicates tumors. *D*, histochemical analysis of the lung with metastatic colonies was performed in the hJAM-C knockdown experiment. EGFP siRNA-transfected and hJAM-C siRNA-transfected HT1080 cells were injected into the tail vein of BALB/c nu/nu mice. After 38 days after implantation, the lung sections were prepared and stained with hematoxylin-eosin. *Scale bars* represent 500 μm. *T* indicates tumors. *L* indicates lymph node. *E*, the influence of hJAM-C knockdown on pulmonary metastasis of HT1080 cells was examined. EGFP siRNA-transfected ($n = 4$, *open circle*) or hJAM-C siRNA-transfected ($n = 4$, *closed circle*) HT1080 cells were injected into the tail vein of BALB/c nu/nu mice. After 38 days after implantation, the weights of lungs were measured as an indicator of pulmonary metastasis. Human JAM-C siRNA-transfection tended to decrease the weight gain of lungs with metastatic colonies when compared with mock transfection ($p = 0.0570$).

confirmed in hJAM-C siRNA-transfected HT1080 cells (Fig. 5*A*). Transfection with hJAM-C siRNA did not affect the rate of cell growth (Fig. 5*B*). In an adhesion assay, the knockdown of hJAM-C inhibited the adhesion of hJAM-C siRNA-transfected HT1080 cells to ECM components (Figs. 4*A* and 5*C*). Especially, the knockdown of hJAM-C significantly reduced their adhesion to fibronectin and vitronectin. The invasion potential of hJAM-C siRNA-transfected HT1080 cells was significantly less than that of luciferase siRNA-transfected HT1080 cells, indicating that the knockdown of hJAM-C reduced tumor invasiveness (Fig. 5*D*).

Finally, the influence of hJAM-C expression on the metastatic potential of HT1080 cells was examined in an experimental metastasis model. The formation of pulmonary metastases was observed in both the Mock/HT1080 cell-injected and the hJAM-C/HT1080 cell-injected group since HT1080 cells are highly metastatic by nature (data not shown). The mean survival times after tumor implantation were 18 ± 2 days for the hJAM-C HT1080 cell-injected group and 30 ± 8 days for the Mock/HT1080 cell-injected group (Fig. 6*A*). The life spans of the hJAM-C/HT1080 cell-injected group were significantly short when compared with those of the Mock/HT1080 cell-injected group ($p < 0.01$). Forced expression of hJAM-C caused 40% reduction of the life span of tumor-bearing mice, suggesting that hJAM-C expression promoted the pulmonary metastasis of HT1080 cells. At 19 days after the injection, the hJAM-C/HT1080 cell-injected group showed bloody lungs with metastatic colonies, which might occur due to the increased malignancy of the metastatic cells (Fig. 6*B*). Most of the mice injected with hJAM-C/HT1080 cells died before showing obvious differences in the lung weight gain between Mock/HT1080 and hJAM-C/HT1080 cell-injected mice. As shown in Fig. 6*C*, the results of the hematoxylin-eosin-staining showed the overexpression of hJAM-C-induced expansion of the metastatic tumors. Histochemical data also showed that the knockdown of hJAM-C in HT1080 cells suppressed the pulmonary metastasis of those cells (Fig. 6*D*). In the case of the injection of EGFP siRNA-transfected cells, the leakages of blood corpuscle cells were observed around the metastases. This phenomenon indicated that the progress of tumor metastasis of the cells transfected with hJAM-C siRNA was slower than that of cells transfected with EGFP siRNA. Furthermore, the knockdown of hJAM-C suppressed the weight gain of lungs with metastatic colonies after the injection of the cells in comparison with that of the cells transfected with EGFP siRNA ($p = 0.0570$, Fig. 6*E*).

DISCUSSION

Invasion of metastatic tumor cells to the secondary colonizing organs is often compared with lymphocyte transendothelial migration since several common cell adhesion molecules, such

as selectins and integrins, are involved in both lymphocyte and tumor cell migration. JAMs are known to participate in the transendothelial migration of lymphocytes (10). Recently, the participation of JAMs in tumor angiogenesis has also been the focus of studies (34, 35). Another recent study demonstrated that JAM-C could mediate tumor cell-endothelial cell interactions and suggested the involvement of JAM-C in tumor cell metastasis (20).

In the present study, to understand the participation of JAM family molecules in tumor metastasis, we first examined the mRNA levels of the JAM family in various cancer cells derived from human and rodent sources. As a result, we observed cell line-dependent differences in the mRNA level of JAM-C. Interestingly, most of the JAM-C-expressing cell lines in this study have often been used for experimental models of metastasis because of their high malignancy. In murine K-1735 melanoma cell lines, the highly metastatic sublines strongly expressed JAM-C when compared with the poorly metastatic ones. In addition, the expression levels of JAM-A and JAM-B on K-1735 cells did not correlate with the metastatic potential of these cells. These data suggested that JAM-C might be implicated in cancer metastasis.

It has been reported that JAM-C shows only 32 and 36% identity to JAM-A and JAM-B, respectively (13). The intracellular region of JAM-C is slightly longer than that of JAM-A and JAM-B (13). The relative tissue distribution of each JAM shows a distinct pattern, resulting from cell type-specific expression of the individual JAM (9). In this study, the unique expression pattern of JAM-C was observed in various cancer cell lines. These observations may explain the distinctive roles of JAM-C in cancer metastasis. The full open reading frame for hJAM-C displays 84% identity with that for murine JAM-C (mJAM-C) at the DNA level and 86% identity at the amino acid level (37). The tissue distribution of hJAM-C does not overlap entirely with that of the murine homologue (13). We also examined mJAM-C function in the invasion assay, with the result that overexpression of mJAM-C also promoted tumor invasion as well as hJAM-C did (data not shown).

In this study, the roles of JAM-C in cancer metastasis were examined by using hJAM-C/HT1080 cells engineered to express hJAM-C abundantly. When compared with Mock/HT1080 cells, these cells showed significantly increased adhesiveness to various ECM components and invasiveness across Matrigel-coated membranes. In addition, the experiments using hJAM-C siRNA showed that endogenous hJAM-C would be involved in tumor adhesion and subsequent invasion. It is not clear whether JAM-C expression enhanced the adhesion of HT1080 cells to various ECM components directly or indirectly. In the case of JAM-A, it has been reported that it regulates β1 integrin expression and cellular adhesion property (36). It is possible that JAM-C may affect the cell adhesiveness by controlling other adhesion molecules. In addition, JAM-C may function cooperatively with certain proteinases since the degradation of Matrigel requires proteinase activity.

Finally, we demonstrated that hJAM-C promoted pulmonary metastasis in the experimental metastatic model *in vivo*. We conclude that the expression of JAM-C promotes cancer metastasis by enhancing the adhesion of and subsequent invasion of cancer cells. The present study is the first report that demonstrates that JAM-C expression promotes tumor malignancy and thus provides a new insight into the mechanisms of cancer metastasis.

REFERENCES

1. Woodhouse, E. C., Chuaqui, R. F., and Liotta, L. A. (1997) *Cancer* **80,** 1529–1537
2. Koike, C., Oku, N., Watanabe, M., Tsukada, H., Kakiuchi, T., Irimura, T., and Okada, S. (1995) *Biochim. Biophys. Acta* **1238,** 99–106
3. Kikkawa, H., Kaihou, M., Horaguchi, N., Uchida, T., Imafuku, H., Takiguchi, A., Yamazaki, Y., Koike, C., Kuruto, R., Kakiuchi, T., Tsukada, H., Takada, Y., Matsuura, N., and Oku, N. (2002) *Clin. Exp. Metastasis* **19,** 717–725
4. Hynes, R. O. (2002) *Nat. Med.* **8,** 918–921
5. Kleiner, D. E., and Stetler-Stevenson, W. G. (1999) *Cancer Chemother. Pharmacol.* **43,** S42–S51
6. Cavallaro, U., and Christofori, G. (2001) *Biochim. Biophys. Acta* **1552,** 39–45
7. Cavallaro, U., and Christofori, G. (2004) *Nat. Rev. Cancer* **4,** 118–132
8. Rojas, M., Fuks, A., and Stanners, C. P. (1990) *Cell Growth Differ.* **1,** 527–533
9. Aurrand-Lions, M., Johnson-Leger, C., Wong, C., Du Pasquier, L., and Imhof, B. A. (2001) *Blood* **98,** 3699–3707
10. Chretien, I., Marcuz, A., Courtet, M., Katevuo, K., Vainio, O., Heath, J. K., White, S. J., and Du Pasquier, L. (1998) *Eur. J. Immunol.* **28,** 4094–4104
11. Liu, Y., Nusrat, A., Schnell, F. J., Reaves, T. A., Walsh, S., Pochet, M., and Parkos, C. A. (2000) *J. Cell Sci.* **113,** 2363–2374
12. Palmeri, D., Van Zante, A., Huang, C. C., Hemmerich, S., and Rosen, S. D. (2000) *J. Biol. Chem.* **275,** 19139–19145
13. Arrate, M. P., Rodriguez, J. M., Tran, T. M., Brock, T. A., and Cunningham, S. A. (2001) *J. Biol. Chem.* **276,** 45826–45832
14. Williams, L. A., Martin-Padura, I., Dejana, E., Hogg, N., and Simmons, D. L. (1999) *Mol. Immunol.* **36,** 1175–1188
15. Santoso, S., Sachs, U. J., Kroll, H., Linder, M., Ruf, A., Preissner, K. T., and Chavakis, T. (2002) *J. Exp. Med.* **196,** 679–691
16. Bazzoni, G., Martinez-Estrada, O. M., Mueller, F., Nelboeck, P., Schmid, G., Bartfai, T., Dejana, E., and Brockhaus, M. (2000) *J. Biol. Chem.* **275,** 30970–30976
17. Liang, T. W., DeMarco, R. A., Mrsny, R. J., Gurney, A., Gray, A., Hooley, J., Aaron, H. L., Huang, A., Klassen, T., Tumas, D. B., and Fong, S. (2000) *Am. J. Physiol.* **279,** C1733–C1743
18. Babinska, A., Kedees, M. H., Athar, H., Ahmed, T., Batuman, O., Ehrlich, Y. H., Hussain, M. M., and Kornecki, E. (2002) *Thromb. Haemostasis* **88,** 843–850
19. Cunningham, S. A., Arrate, M. P., Rodriguez, J. M., Bjercke, R. J., Vanderslice, P., Morris, A. P., and Brock, T. A. (2000) *J. Biol. Chem.* **275,** 34750–34756
20. Santoso, S., Orlova, V. V., Song, K., Sachs, U. J., Andrei-Selmer, C. L., and Chavakis, T. (2005) *J. Biol. Chem.* **280,** 36326–36333
21. Ostermann, G., Weber, K. S., Zernecke, A., Schroder, A., and Weber, C. (2002) *Nat. Immunol.* **3,** 151–158
22. Cunningham, S. A., Rodriguez, J. M., Arrate, M. P., Tran, T. M., and Brock, T. A. (2002) *J. Biol. Chem.* **277,** 27589–27592
23. Bazzoni, G., Martinez-Estrada, O. M., Orsenigo, F., Cordenonsi, M., Citi, S., and Dejana, E. (2000) *J. Biol. Chem.* **275,** 20520–20526
24. Ebnet, K., Schulz, C. U., Meyer, Zu Brickwedde, M. K., Pendl, G. G., and Vestweber, D. (2000) *J. Biol. Chem.* **275,** 27979–27988
25. Martinez-Estrada, O. M., Villa, A., Breviario, F., Orsenigo, F., Dejana, E., and Bazzoni, G. (2001) *J. Biol. Chem.* **276,** 9291–9296
26. Ebnet, K., Suzuki, A., Horikoshi, Y., Hirose, T., Meyer Zu Brickwedde, M. K., Ohno, S., and Vestweber, D. (2001) *EMBO J.* **20,** 3738–3748
27. Itoh, M., Sasaki, H., Furuse, M., Ozaki, H., Kita, T., and Tsukita, S. (2001) *J. Cell Biol.* **154,** 491–497
28. Hamazaki, Y., Itoh, M., Sasaki, H., Furuse, M., and Tsukita, S. (2002) *J. Biol. Chem.* **277,** 455–461

29. Vestweber, D. (2002) *Curr. Opin. Cell Biol.* **14,** 587–593
30. Chavakis, T., Preissner, K. T., and Santoso, S. (2003) *Thromb. Haemostasis* **89,** 13–17
31. Muller, W. A. (2002) *Lab. Investig.* **5,** 521–533
32. Yamakawa, S., Furuyama, Y., and Oku, N. (2000) *Biol. Pharm. Bull.* **23,** 1264–1266
33. Fidler, I. J., Gruys, E., Cifone, M. A., Barnes, Z., and Bucana, C. (1981) *J. Natl. Cancer Inst.* **67,** 947–956
34. Naik, M. U., Mousa, S. A., Parkos, C. A., and Naik, U. P. (2003) *Blood* **102,** 2108–2114
35. Lamagna, C., Hodivala-Dilke, K. M., Imhof, B. A., and Aurrand-Lions, M. (2005) *Cancer Res.* **65,** 5703–5710
36. Mandell, K. J., Babbin, B. A., Nusrat, A., and Parkos, C. A. (2005) *J. Biol. Chem.* **280,** 11665–16674
37. Johnson-Leger, C. A., Aurrand-Lions, M., Beltraminelli, N., Fasel, N., and Imhof, B. A. (2002) *Blood* **100,** 2479–2486

Journal of Medical Virology 79:977–986 (2007)

Anti-HTLV-1 Tax Antibody and Tax-Specific Cytotoxic T Lymphocyte Are Associated With a Reduction in HTLV-1 Proviral Load in Asymptomatic Carriers

Masaki Akimoto,[1] Tomohiro Kozako,[2] Takashi Sawada,[3] Kakushi Matsushita,[1] Atsuo Ozaki,[1] Heiichiro Hamada,[1] Hideaki Kawada,[1] Makoto Yoshimitsu,[1] Masahito Tokunaga,[1] Koichi Haraguchi,[1] Kimiharu Uozumi,[2] Naomichi Arima,[2]* and Chuwa Tei[4]

[1]*Department of Hematology and Immunology, Kagoshima University Hospital, Kagoshima, Japan*
[2]*Division of Host Response, Center for Chronic Viral Diseases, Kagoshima University Graduate School of Medical and Dental Sciences, Kagoshima, Japan*
[3]*Clinical Research Center, Eisai Co., Ltd., Tokyo, Japan*
[4]*Department of Cardiovascular, Respiratory and Metabolic Medicine, Kagoshima University Graduate School of Medical and Dental Sciences, Kagoshima, Japan*

Previous studies have suggested that higher anti-human T-lymphotropic virus 1 (HTLV-1) antibody titer and lower anti-HTLV-1 Tax antibody reactivity are risk factors for adult T-cell leukemia/lymphoma. In the present study, we analyzed the relationships between these factors and clarified their significance. Forty-five carriers were examined for anti-HTLV-1 and anti-Tax antibody by ELISA. In addition, 43 of the 45 carriers with HLA-A*0201 and/or A*2402 were examined for frequency of Tax-specific cytotoxic T lymphocytes (CTLs) using HTLV-1/HLA tetramers, and 44 were examined for proviral load by real-time PCR. The relationships between these factors were analyzed statistically. The frequencies of Tax11-19 and Tax301-309-specific CTLs were significantly higher in the anti-Tax antibody-positive group as compared with the antibody-negative group ($P=0.002$ and 0.033, respectively). Anti-HTLV-1 antibody titer had a positive correlation with proviral load ($P=0.019$), whereas anti-Tax antibody did not show a significant correlation. Higher frequencies of both Tax11-19 and Tax301-309-specific CTLs are related to a reduction in proviral load ($P=0.017$ and 0.015, respectively). Synergistic interactions of humoral and cellular immunity against Tax protein were demonstrated in HTLV-1 carriers. Tax-specific CTL may reduce HTLV-1 proviral load to prevent asymptomatic carriers from developing adult T-cell leukemia/lymphoma. ***J. Med. Virol. 79:977–986, 2007.***

KEY WORDS: anti-Tax antibody; CTL; HTLV-1; proviral load; carrier

INTRODUCTION

Human T-lymphotropic virus 1 (HTLV-1) is a strain in the genus *Deltaretrovirus*, family *Retroviridae*. It is etiologically linked to adult T-cell leukemia/lymphoma [Poiesz et al., 1980; Hinuma et al., 1981] and a chronic inflammatory neurological disorder designated HTLV-1-associated myelopathy/tropical spastic paraparesis (HAM/TSP) [Gessain et al., 1985; Osame et al., 1986]. HTLV-1 is prevalent in Japan, the Caribbean, South America, Africa, Melanesia, and the Middle East [Maloney and Blattner, 2003]. In Japan, it is estimated that approximately 1 million people are infected with HTLV-1, and most HTLV-1 carriers are asymptomatic throughout their lives. However, 1–5% of infected individuals develop adult T-cell leukemia/lymphoma [Tajima, 1990], and less than 1% develop HAM/TSP or other inflammatory disorders.

Although adult T-cell leukemia/lymphoma is caused by HTLV-1 infection, generally a long latent period about 60 years is needed for the development of the disease after initial infection mainly via breastfeeding [Hino et al., 1985; Kinoshita et al., 1987]. The Miyazaki Cohort Study of HTLV-1 carriers suggested that the

Grant sponsor: Japanese Ministry of Health, Labour, and Welfare; Grant sponsor: Kagoshima University for Frontier Science Research Center Program.

*Correspondence to: Naomichi Arima, Division of Host Response, Center for Chronic Viral Diseases, Kagoshima University Graduate School of Medical and Dental Sciences, 8-35-1 Sakuragaoka, Kagoshima 890-8544, Japan.
E-mail: nao@m2.kufm.kagoshima-u.ac.jp

Accepted 14 December 2006
DOI 10.1002/jmv.20807
Published online in Wiley InterScience (www.interscience.wiley.com)

risk factors for the development of adult T-cell leukemia/lymphoma from carriers include vertical HTLV-1 infection, gender (male > female), and increased numbers of abnormal lymphocytes (Ably) [Hisada et al., 1998a, 2001]. Others have reported that the percentage of circulating Ably are strongly correlated with HTLV-1 proviral load [Hisada et al., 1998a; Tachibana et al., 1992]. Moreover, persistent proliferation of HTLV-1-infected $CD4^+$ T-cell clones in asymptomatic carriers is accompanied with a high proviral load [Etoh et al., 1997]. These observations suggest that high HTLV-1 proviral load is also correlated with a risk of the development of adult T-cell leukemia/lymphoma.

Anti-HTLV-1 antibody is detected in all HTLV-1-infected individuals, either asymptomatic carriers or patients with HTLV-1-associated diseases. In the Miyazaki Cohort Study, a higher anti-HTLV-1 antibody titer was a high risk factor for the development of adult T-cell leukemia/lymphoma [Hisada et al., 1998b]. In contrast, a lower prevalence of antibody to Tax protein (anti-Tax antibody) has been demonstrated in patients with adult T-cell leukemia/lymphoma compared with asymptomatic HTLV-1 carriers [Yokota et al., 1989]. A lower prevalence of anti-Tax antibody has also been demonstrated in a subset of HTLV-1 carriers with detectable levels of Ably (>0.6%) [Hisada et al., 1998a], suggesting that anti-Tax antibody reactivity is low among patients with adult T-cell leukemia/lymphoma before their clinical diagnosis. Anti-Tax antibody levels in all five subjects who developed adult T-cell leukemia/lymphoma were low for up to 10 years preceding their diagnosis in the cohort study. These findings suggest that a lower anti-Tax antibody level is a significant risk factor for the development of adult T-cell leukemia/lymphoma [Hisada et al., 1998b].

Recently, HTLV-1-specific cytotoxic T lymphocytes (CTLs) have attracted a great deal of attention with regard to host immunity against infection with the virus. HTLV-1 Tax protein is the most common target for HTLV-1-specific CTLs in infected individuals [Jacobson et al., 1990; Kannagi et al., 1991]. Tax-specific CTLs can be induced from peripheral blood mononuclear cells (PBMCs) of asymptomatic carriers in vitro. In contrast, induction of Tax-specific CTLs is rarely observed in PBMCs of patients with adult T-cell leukemia/lymphoma [Kannagi et al., 1983, 1984, 1993, 1994; Jacobson et al., 1990; Parker et al., 1992]. The insufficient Tax-specific CTL response in patients with adult T-cell leukemia/lymphoma suggests that these CTLs contribute to surveillance for the disease in HTLV-1-infected individuals.

On the other hand, previous studies have suggested that HTLV-1 proviral load is also a major risk factor for HAM/TSP; the median proviral load is 16-fold higher in HAM/TSP patients than in healthy carriers [Nagai et al., 1998]. A high HTLV-1 proviral load is also associated with an increased risk of progression to disease [Nagai et al., 1998; Taylor et al., 1999].

These findings suggest that a reduction in HTLV-1 proviral load in circulating lymphocytes prevents HTLV-1 carriers from contracting adult T-cell leukemia/lymphoma and HAM/TSP. Although anti-HTLV-1 antibody, anti-Tax antibody, and Tax-specific CTLs seem to be related to HTLV-1 proviral load and the development of HTLV-1-associated diseases, the details are poorly understood. In the present study, we demonstrated relationships between anti-HTLV-1 antibody, anti-Tax antibody, Tax-specific CTLs, and HTLV-1 proviral load, and discuss the risk factors for the development of adult T-cell leukemia/lymphoma and HAM/TSP.

MATERIALS AND METHODS

Subjects and PBMCs

The study population consisted of 45 asymptomatic carriers who visited Kagoshima University Hospital for examination to determine HTLV-1 carrier state and for a clinical check-up during the period from September 2004 to May 2005. None of the subjects had clinical signs, symptoms, or HTLV-1-associated diseases. Informed consent was obtained from all subjects and the study protocol was reviewed and approved by the Medical Ethical Committee of Kagoshima University. Blood samples obtained at clinical visits were collected in EDTA tubes for determination of the complete blood counts and differential counts using standard methods. Ably were counted by a hematologist during microscopic review of peripheral blood smears, which were fixed in methanol and stained with Giemsa. Ably were identified according to the criteria reported previously [Kondo et al., 1985]. The number of Ably among 100 leukocytes was recorded as a percentage. PBMCs were separated from heparinized whole blood by centrifugation on Ficoll/Hypaque (Pharmacia, Uppsala, Sweden). For subsequent experiments, the cells were cryopreserved in liquid nitrogen until assayed as described previously [Katahira et al., 1995].

HLA Typing of PBMCs

In our recent study, analysis of HLA type revealed that more than 80% of asymptomatic HTLV-1 carriers and patients with adult T-cell leukemia/lymphoma had HLA-A*02 or HLA-A*24 [Kozako et al., 2006], consistent with other reports of HLA allele types in the population of Southern Kyushu [Sonoda, 2003]. HLA types were determined by serological tests using monoclonal antibodies (mAbs) for HLA-A*02 (clone: BB7.2) and HLA-A*24 (clone: 17A10; kindly provided by Medical and Biological Laboratories, Nagoya, Japan). Indirect staining was completed by incubation of cells with goat anti-mouse IgG-fluorescein isothiocyanate (FITC) (Immunotech, Miami, FL). HLA allele types were also confirmed by the Luminex method using DNA isolated from the cryopreserved PBMCs as described (G & G Science, Fukushima, Japan) [Kikkawa et al., 2003].

Tetramer Assay for HTLV-1-Specific CTL

We used 14 distinct phycoerythrin (PE)-conjugated HLA-A*0201 and HLA-A*2402 tetramers for HTLV-1

Tax and Env peptides (Medical and Biological Laboratories) in reference to the previous HTLV-1 Tax and Env CTL epitope mapping data [Yashiki et al., 2001]. In addition, two HTLV-1/HLA tetramers were purchased from Beckman Coulter (Fullerton, CA). Finally, 16 HTLV-1/HLA tetramers were prepared for the present study. The 16 epitopes were as follows: Tax11-19 (LLFGYPVYV), Tax123-131 (TLGQHLPTL), Tax155-163 (YLYQLSPPI), Tax178-186 (QLGAFLTNV), Tax307-315 (LLFEEYTNI), Env175-183 (FLNTEPSQL), Env239-247 (VLYSPNVSV), and Env442-450 (ALQTGITLV) for HLA-A*0201, Tax12-20 (LFGYPVYVF), Tax187-195 (PYKRIEELL), Tax289-297 (SFLLSHGLI), Tax301-309 (SFHSLHLLF), Tax311-319 (EYTNIPISL), Env11-19 (FFQFCPLIF), Env21-29 (DYSPSCCTL), and Env153-161 (HFSKCGFPF) for HLA-A*2402 (anchor motifs are indicated in boldface). The quality of each HLA-tetramer was tested by HPLC and biological assay for respective CTLs. Aliquots of 1×10^6 freshly isolated PBMCs were reacted with the 16 HLA tetramers for 45 min at 4°C with FITC-conjugated mouse anti-human CD8 mAbs according to the manufacturer's instructions (Medical and Biological Laboratories). All samples were also examined for surface markers using mouse anti-CD4-PE (Beckman Coulter) and anti-CD45-Peridinin Chlorophyll-a Protein (Becton Dickinson, San Jose, CA). Aliquots of 1×10^5 CD45-positive lymphocytes in fresh samples were analyzed on a FACScan using CellQuest software (Becton Dickinson) [Bieganowska et al., 1999; Kuzushima et al., 2001].

Detection of Anti-HTLV-1 and Anti-Tax Antibody

Anti-HTLV-1 antibody titer and anti-Tax antibody reactivity were examined in the 45 subjects. Anti-HTLV-1 antibody was measured by electrochemiluminescence immunoassay (ECLIA) (Picolumi®HTLV-I; Eisai, Tokyo, Japan) in our hospital, using beads coated with purified HTLV-1 antigen and synthetic Env peptides. Anti-Tax antibody was measured by ELISA, using a recombinant Tax protein expressed in *Escherichia coli* with a full-length HTLV-1 tax gene. The cut-off value was determined from the average of the ELISA absorbance value plus three SD obtained from 169 specimens negative for anti-Tax antibody (Eisai) [Kamihira et al., 1989; Sawada et al., 1989; Kashiwagi et al., 1990]. The levels of antibodies were estimated using a cut-off index (CI): the corresponding serum was considered ELISA-positive at $CI \geq 1.1$.

Real-Time PCR Quantitation of HTLV-1 Proviral Load in PBMCs

The standard HTLV-1 DNA was prepared from MT-2 cells [Miyoshi et al., 1981]. Real-time PCR quantitation of HTLV-1 DNA was performed in a Light-Cycler System (Roche Diagnostics, Mannheim, Germany) using measurements of 12 test samples with standard DNA for each assay. The HTLV-1 primer set corresponded to the highly conserved HTLV-1 pX region, SK43, and SK44 [Ehrlich et al., 1990]. The HTLV-1 pX probe set was designed for the two adjacent parts of the pX region, which were labeled with different fluorophores [Sonoda et al., 2004].

The HTLV-1 proviral load was expressed as number of copies per 1,000 cells using the following formula: HTLV-1 proviral load = [(HTLV-1 pX copy number)/(β-globin copy number/2)] × 1,000. The limit of detection of this method was 0.2 copies of HTLV-1 provirus/1,000 cells. Real-time PCR quantitation of HTLV-1 provirus DNA has an inherent error of 25% in terms of coefficient of variation (CV), as seen in different inter-assay runs for HTLV-1 proviral load [Nagai et al., 1998]. However, the present real-time PCR quantitation with duplicate intra-assay reduced the CV to less than 8% [Sonoda et al., 2004]. Using this method, we could perform accurate measurements of HTLV-1 proviral load in PBMCs of asymptomatic HTLV-1 carriers.

Statistical Analysis

Correlation analyses were performed based on either Pearson or Spearman's rho correlation coefficients as appropriate. The resulting values for the two subject groups were compared with Mann–Whitney U tests. SPSS for Windows (version 14.0J; SPSS, Inc., Chicago, IL) was used for statistical analysis, and $P < 0.05$ was considered significant.

RESULTS

Characteristics of the Subjects

The age, sex, and HTLV-1-related markers of these 45 asymptomatic carriers (18 men and 27 women) are summarized in Table I. The subjects' median age was 58 years old with a range from 22 to 82. The median leukocyte count was 5,200/μl with a range from 1,900 to 9,500, and the median Ably level was 1% with a range from 0 to 6% (data not shown). In the present study, overt adult T-cell leukemia/lymphoma, including smoldering type, was excluded by Southern blot hybridization of HTLV-1 proviral DNA. The two cases with Ably levels of more than 5% in the present study (case #12, 6%; case #36, 5%) were also diagnosed as carriers, as no band was detected by Southern blot hybridization.

All 45 cases were positive for anti-HTLV-1 antibodies, and the titers ranged from 2.8 to 330.9 CI with a median value of 81.6. On the other hand, anti-Tax antibody was found in 15 of the 45 cases (33%). One subject (case #43) could not be included in the HTLV-1 proviral load analysis, as his PBMCs were no longer available. The median proviral load was 62.3/1,000 copies ranging from 4.6 to 592.4.

Ten of the 45 carriers had HLA-A*0201, 25 had HLA-A*2402, 8 had both alleles in heterozygous combination, and 2 had neither HLA-A*0201 nor HLA-A*2402. As the HLA-tetramers in the present study can detect HTLV-1-specific $CD8^+$ cells possessing either HLA-A*0201 or HLA-A*2402, 43 cases were examined for

TABLE I. HTLV-1-Related Markers Among the 45 Asymptomatic Carriers

Case No.	Age	Sex	Anti-HTLV-1 antibody titer (CI)	Anti-Tax antibody titer (CI)	Anti-Tax antibody positivity	Tax11-19-specific CTL (%)	Tax301-309-specific CTL (%)	Proviral load (/1,000 copies)
HLA-A*0201-related								
1	72	F	5.5	0.21	−	0.03	NA	21.0
2	74	M	23.71	0.24	−	0.00	NA	12.2
3	46	F	6.1	0.21	−	0.08	NA	24.1
4	53	M	41.8	1.79	+	0.29	NA	39.7
5	47	F	16.8	0.68	−	0.00	NA	71.8
6	56	F	141.5	0.29	−	0.00	NA	17.3
7	54	M	30.92	7.25	+	0.09	NA	63.2
8	66	F	2.9	0.26	−	0.00	NA	25.1
9	51	F	225.6	0.61	−	0.00	NA	128.7
10	62	F	20.46	0.82	−	0.01	NA	9.8
HLA-A*0201 and HLA-A*2402-related								
11	80	F	20.0	1.71	+	0.73	0.07	42.7
12	63	M	282.4	0.71	−	0.02	0.23	469.3
13	70	F	89.47	0.26	−	0.03	0.02	135.4
14	47	F	30.1	0.29	−	0.00	0.00	12.2
15	61	F	37.8	0.29	−	0.04	0.00	5.2
16	72	F	23.5	0.40	−	0.00	0.00	22.4
17	62	F	2.8	1.24	+	0.14	0.04	4.6
18	53	M	145.7	1.61	+	0.03	0.01	4.8
HLA-A*2402-related								
19	58	F	256.4	1.76	+	NA	0.16	106.9
20	52	M	81.6	0.29	−	NA	0.50	61.4
21	47	M	142.8	0.24	−	NA	0.14	69.5
22	51	F	70.8	0.29	−	NA	0.00	338.3
23	22	F	198.0	2.71	+	NA	1.11	93.7
24	68	F	101.5	0.35	−	NA	0.00	79.8
25	69	F	241.5	0.29	−	NA	0.00	271.2
26	80	F	288.8	6.82	+	NA	0.55	82.3
27	53	F	117.1	0.35	−	NA	0.06	592.4
28	58	F	101.2	0.32	−	NA	0.15	107.3
29	82	M	39.85	0.74	−	NA	0.12	26.1
30	68	F	76.46	5.85	+	NA	0.00	27.3
31	66	F	12.25	0.21	−	NA	0.31	54.6
32	68	M	147.39	0.50	−	NA	0.17	213.4
33	31	M	159.4	0.29	−	NA	0.47	69.5
34	73	M	62.8	0.48	−	NA	0.15	77.9
35	55	F	139.71	6.75	+	NA	1.05	73.2
36	58	M	231.7	2.14	+	NA	1.37	27.0
37	57	M	11.1	2.25	+	NA	0.19	11.4
38	70	F	330.9	5.01	+	NA	3.25	40.4
39	44	M	46.0	0.72	−	NA	0.01	144.5
40	78	M	73.6	0.54	−	NA	0.19	50.9
41	61	M	95.4	2.43	+	NA	0.16	68.4
42	76	F	169.42	1.52	+	NA	0.41	41.0
43	58	F	76.34	0.91	−	NA	0.60	NA
Irrelevant HLA alleles								
44	43	M	121.2	0.18	−	NA	NA	97.1
45	53	M	162.5	0.26	−	NA	NA	265.9

NA, not available.

each tetramer-CD8$^+$ cells. The cases with more than 0.03% tetramer-CD8$^+$ cells distributed as a cluster were judged as positive for HTLV-1-specific CD8$^+$ cells in the present study. Most subjects had single epitope-specific CTLs for each HLA allele: Tax11-19-specific CTL for HLA-A*0201 and Tax301-309-specific CTL for HLA-A*2402. A few subjects had multiple epitope-specific CTLs for one HLA allele, including the major epitope-specific CTLs mentioned above and a few minor epitope-specific CTLs. In the present study, we assessed only the major CTLs in both HLA alleles, as shown in Table I. Nine of the 18 (50%) cases with HLA-A*0201 were positive for Tax11-19-specific CTLs, and 23 of the 33 (69.7%) cases with HLA-A*2402 were positive for Tax301-309-specific CTLs. Only two cases (case #16: 0.08% and case #35: 0.06%) had sufficient Env-specific CTLs.

Relationships Between HTLV-1-Related Markers

Anti-HTLV-1 antibody titer in the anti-Tax antibody-positive group was not different from that in the

antibody-negative group (median 139.7 vs. 75.0, $P=0.194$, Mann–Whitney; Fig. 1). There was no significant correlation between anti-HTLV-1 antibody titer and the frequency of Tax11-19-specific CTLs ($P=0.628$, Spearman; Fig. 2A), whereas the frequency of Tax11-19-specific CTLs was significantly higher in the anti-Tax antibody-positive group compared with the antibody-negative group among HLA-A*0201-positive cases (median 0.14 vs. 0.00%, $P=0.002$, Mann–Whitney; Fig. 2B). On the other hand, there was a significant positive correlation between anti-HTLV-1 antibody titer and the frequency of Tax301-309-specific CTLs ($r=0.549$, $P=0.001$, Pearson; Fig. 2C), and the frequency of Tax301-309-specific CTLs was also significantly higher in the anti-Tax antibody-positive group compared with the antibody-negative group among HLA-A*2402-positive cases (median 0.19 vs. 0.09%, $P=0.033$, Mann–Whitney; Fig. 2D).

There was a significant positive correlation between anti-HTLV-1 antibody titer and HTLV-1 proviral load ($r=0.353$, $P=0.019$, Pearson; Fig. 3A). However, the proviral load in the anti-Tax antibody-positive group was not different from and even seemed slightly lower than that in the antibody-negative group (median 41.0 vs. 69.5/1,000 copies, $P=0.147$, Mann–Whitney; Fig. 3B). Next, we analyzed the relationship between Tax-specific CTLs and proviral load. As shown in Figure 4, the frequency of Tax11-19-specific CTLs was significantly lower than that of Tax301-309-specific CTLs (the frequencies of Tax301-309-specific CTLs in Tax11-19-specific CTL-positive carriers were excluded previously) in the CTL-positive carriers (median 0.08 vs. 0.19%, $P=0.009$, Mann–Whitney). However, the proviral load in the Tax11-19-specific CTL-positive group was significantly lower than that in the Tax11-19-specific CTL-negative group consisting of cases with Tax301-309-specific CTL alone or neither CTL (median 24.1 vs. 69.5/1,000 copies, $P=0.017$, Mann–Whitney; Fig. 5A). On the other hand, the proviral load in the Tax301-309-specific CTL-positive group was not different from that in the CTL-negative group consisting of cases with Tax11-19-specific CTL alone or neither CTL (median 69.0 vs. 33.5/1,000 copies, $P=0.291$, Mann–Whitney; Fig. 5B). The reason that the Tax301-309-specific CTL-positive group did not have lower proviral load than the CTL-negative group can be explained by the inclusion in the Tax301-309-specific CTL-negative group of many cases with Tax11-19-specific CTLs as very strong negative regulators of HTLV-1 proviral load (7 of 22 carriers) [Jeffery et al., 1999, 2000; Nagai et al., 2001; Vine et al., 2002; Yao et al., 2006]. Therefore, we next analyzed the relationship between Tax301-309-specific CTLs and proviral load among cases positive for HLA-A*2402 but not A*0201. These subjects were divided into a higher Tax301-309-specific CTL frequency group (>median: 0.17%, n = 11; case #43 was not included as mentioned above) and a lower CTL frequency group (≤0.17%, n = 13), and the proviral load in the former was significantly lower than that in the latter (median 54.6 vs. 106.9/1,000 copies, $P=0.015$, Mann–Whitney; Fig. 6).

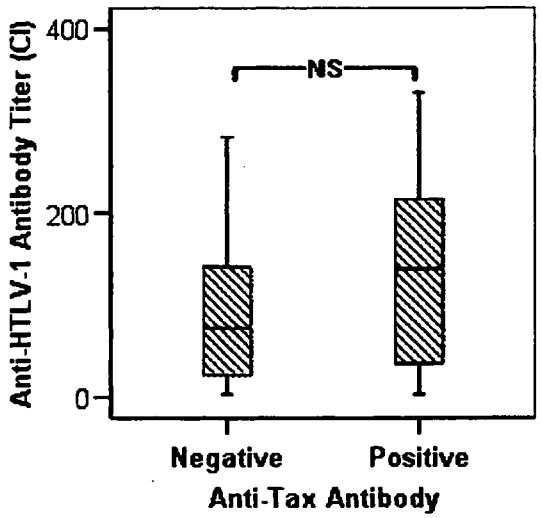

Fig. 1. Comparison of anti-HTLV-1 antibody titer between the anti-Tax antibody-positive and negative groups. Anti-HTLV-1 antibody titer in the anti-Tax antibody-positive group was not different from that in the antibody-negative group (median 139.7 vs. 75.0, $P=0.194$, Mann–Whitney).

DISCUSSION

The present study was performed to examine the relationships between anti-HTLV-1 antibody, anti-Tax antibody, Tax-specific CTLs, and HTLV-1 proviral load in asymptomatic carriers. Anti-HTLV-1 antibody is predominantly directed against structural polypeptides of HTLV-1, such as Env or Gag, but rarely against Tax [Yamamoto et al., 1983; Schneider et al., 1984]. Therefore, it is likely that anti-HTLV-1 and anti-Tax antibodies are each controlled by independent regulation of production. We found no significant correlation between anti-Tax antibody positivity and anti-HTLV-1 antibody titer in the present study (Fig. 1). On the other hand, the frequency of Tax11-19-specific CTLs showed a significant positive correlation only with anti-Tax antibody positivity, but not with anti-HTLV-1 antibody titer, although the frequency of Tax301-309-specific CTLs showed significant positive correlations with both types of antibody (Fig. 2). These findings imply that anti-Tax antibody is associated with Tax-specific CTLs, and suggest a strong positive correlation between humoral and cellular immunity against HTLV-1 Tax. A recent study demonstrated that long-lasting $CD4^+$ T-cell memory depends on the presence of B cells retaining antigen [van Essen et al., 2000]. Furthermore, polyclonal activation of B cells may help to optimize the memory CTL response against persistent viruses that are predominantly controlled by CTL [Matter et al., 2005]. These mechanisms may help explain the close relationship between the anti-Tax antibody and the frequency of Tax-specific CTLs that we report here. Perhaps anti-Tax antibody can serve as a convenient marker for the presence of Tax-specific CTLs.

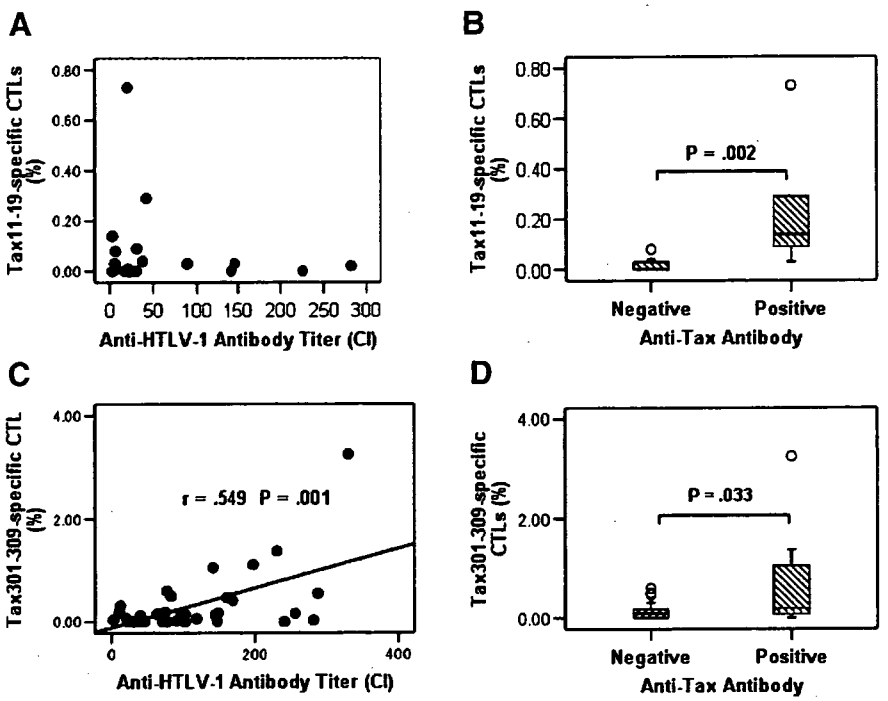

Fig. 2. . Relationships between the frequencies of Tax-specific CTLs and anti-HTLV-1 or anti-Tax antibody. There was no significant correlation between anti-HTLV-1 antibody titer and the frequency of Tax11-19-specific CTLs ($P = 0.628$, Spearman) (**A**), whereas the frequency of Tax11-19-specific CTLs was significantly higher in the anti-Tax antibodypositive group compared with the antibody-negative group among HLA-A*0201-positive cases (median 0.14 vs. 0.00%, $P = 0.002$, Mann–Whitney) (**B**). There was a significant positive correlation between anti-HTLV-1 antibody titer and the frequency of Tax301-309-specific CTLs ($r = 0.549$, $P = 0.001$, Pearson) (**C**), and the frequency of Tax301-309-specific CTLs was also significantly higher in the anti-Tax antibody-positive group compared with the antibody-negative group among HLA-A*2402-positive cases (median 0.19 vs. 0.09%, $P = 0.033$, Mann–Whitney) (**D**).

As predicted from the findings of the Miyazaki Cohort Study [Ishihara et al., 1994], we found a strong positive correlation between anti-HTLV-1 antibody and HTLV-1 proviral load among asymptomatic carriers. However, it remains unclear whether this high antibody titer contributes significantly to controlling the equilibrium proviral load. We observed very few Env-specific CTLs in asymptomatic carriers which further suggests insufficient collaboration of humoral and cellular immunity against Env protein. The positive relationship between anti-HTLV-1 antibody and proviral load can be explained by induction of high anti-HTLV-1 antibody titer in response to a high proviral load. In the absence of sufficient virus-specific CTLs, however, the proviral load remains elevated. In contrast, a tendency toward a negative relationship between the anti-Tax antibody positivity and the proviral load is hinted at in our studies, although statistical analysis did not show a significant correlation between these factors (Fig. 3).

The observed relationship between anti-Tax antibody titer and the proviral load can be explained by presence of high frequency of CTLs against HTLV-1 Tax in anti-Tax antibody-positive carriers. Tax11-19-specific CTLs showed a strong negative relationship to the proviral load (Fig. 5A), and Tax301-309-specific CTLs also showed a negative relationship to that after exclusion of the bias due to Tax11-19-specific CTLs (Fig. 6). As carriers with higher anti-Tax antibody titer will have a higher frequency of Tax-specific CTLs, as demonstrated above, anti-Tax antibody may play a role in reducing proviral load indirectly, although it will not kill the virus-infected cells directly.

Previous studies have strongly suggested that elevated proviral loads are closely related with the development of adult T-cell leukemia/lymphoma [Kinoshita et al., 1985; Yokota et al., 1989; Manns et al., 1999; Taylor et al., 1999; Okayama and Stuver, 2003]. Our findings also indicate that HTLV-1 carriers from the Miyazaki Cohort Study with the highest anti-HTLV-1 antibody titers and lowest anti-Tax antibody reactivity may be at greatest risk for adult T-cell leukemia/lymphoma.

On the other hand, previous studies have suggested that CTLs may be useful to determine the proviral load and the risk of proinflammatory disease [Bangham et al., 1996, 1999]. It is possible that HTLV-1-specific CTLs exert both protective and inflammatory effects. There is also evidence that HTLV-1-specific CTL may contribute to the inflammation seen in HAM/TSP [Elovaara et al., 1993; Ijichi et al., 1993; Biddison et al., 1997; Levin et al., 1997; Kubota et al., 1998]. However, frequent and chronically activated HTLV-1-specific CTLs have been found in healthy carriers as well as in HAM/TSP patients [Parker et al., 1992, 1994; Daenke et al., 1996; Jeffery et al., 1999]. Therefore, previous studies suggested that the CTLs efficiently destroy HTLV-1-infected cells *in vivo* and thus protect against inflammatory diseases, such as HAM/TSP

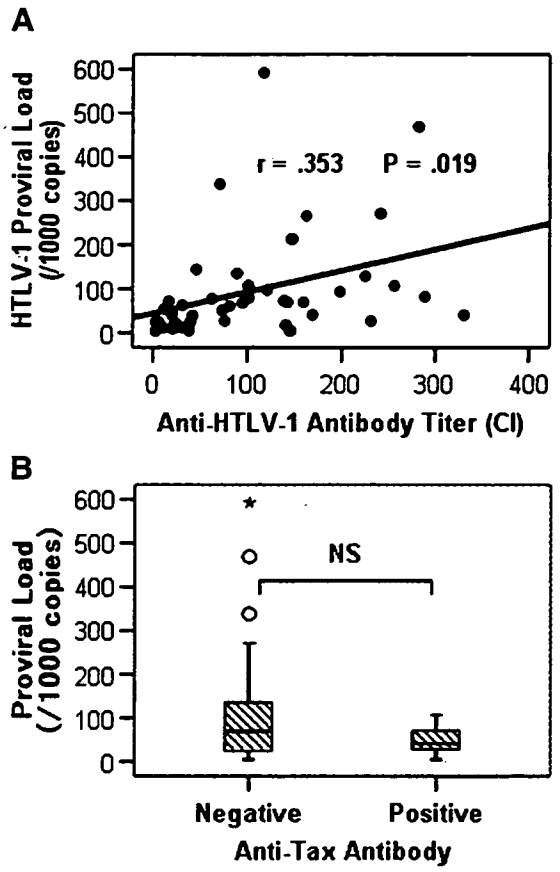

Fig. 3. Relationships between HTLV-1 proviral load and anti-HTLV-1 or anti-Tax antibody. There was a significant positive correlation between anti-HTLV-1 antibody titer and HTLV-1 proviral load ($r = 0.353$, $P = 0.019$, Pearson) (**A**). However, the proviral load in the anti-Tax antibody-positive group was not different from and seemed slightly lower than that in the antibody-negative group (median 41.0 vs. 69.5/1,000 copies, $P = 0.147$, Mann–Whitney) (**B**).

[Niewiesk et al., 1994; Hanon et al., 2000]. In addition, a recent case-control study showed that the MHC class I genes HLA-A*02 and/or Cw*08 conferred protection against HAM/TSP; possession of the A*02 and/or Cw*08 genes prevented 36% of potential HAM/TSP cases [Jeffery et al., 1999, 2000]. These observations suggested that both A*02 and Cw*08-restricted CTLs are particularly efficient at recognizing Tax, and reduce the proviral load and hence the risk of disease. In our study, Tax11-19-specific CTLs showed a negative relationship to the proviral load more strongly than Tax301-309-specific CTLs (Fig. 5). This result favors the conclusion of the previous study that demonstrated a protective effect of HLA-A*02 against HTLV-1 proviral load and the risk of HAM/TSP in virus-infected individuals, as the Tax11-19-specific CTLs are HLA-A*0201-restricted [Jeffery et al., 1999]. Tax11-19-specific CTLs will proliferate rapidly in response to HTLV-1 Tax, and kill HTLV-1-infected cells rapidly, and so limit the proviral load to a low level. However, the proliferation rate of the CTLs will not be stimulated to a greater extent by the proviral load when a strong immune response reaches equilibrium with a low

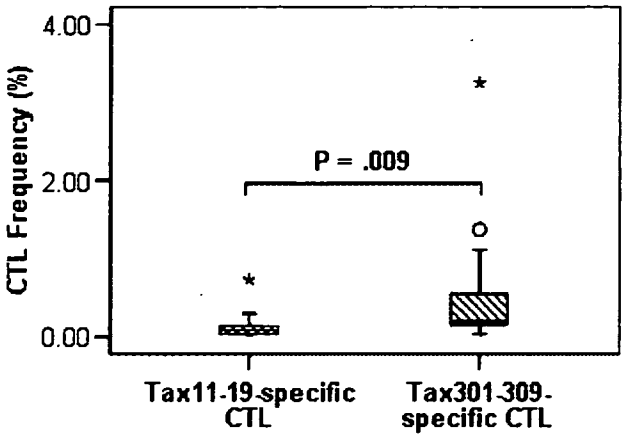

Fig. 4. Comparison of the frequencies between Tax11-19 and Tax301-309-specific CTLs. The frequency of Tax11-19-specific CTLs was significantly lower than that of Tax301-309-specific CTLs in the CTL-positive carriers (median 0.08 vs. 0.19%, $P = 0.009$, Mann–Whitney). The frequencies of Tax301-309-specific CTLs in Tax11-19-specific CTL-positive carriers were excluded previously.

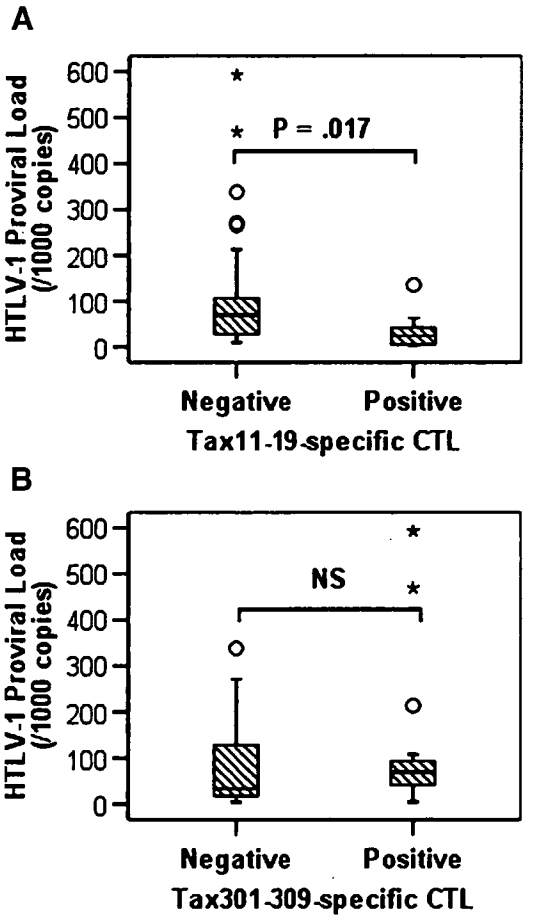

Fig. 5. Comparison of HTLV-1 proviral load between Tax-specific CTL-positive and CTLnegative groups. HTLV-1 proviral load was significantly lower in the Tax11-19-specific CTL-positive group compared with the CTL-negative group among all cases (median 24.1 vs. 69.5, $P = 0.017$, Mann–Whitney) (**A**). On the other hand, proviral load was not different between Tax301-309-specific CTL-positive and CTL-negative groups (median 69.0 vs. 33.5/1,000 copies, $P = 0.291$, Mann–Whitney) (**B**).

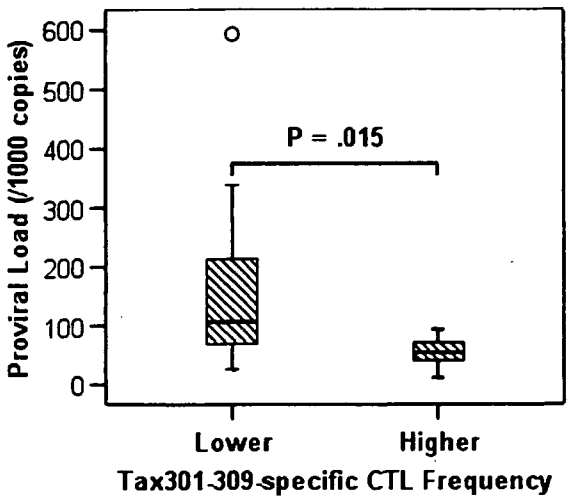

Fig. 6. Comparison of HTLV-1 proviral load between groups with higher and lower frequencies of Tax301-309-specific CTLs. HTLV-1 proviral load was significantly lower in the group with higher frequency of Tax301-309-specific CTLs (>0.17%) compared with the group with lower frequency of these CTLs (≤0.17%) (median 54.6 vs. 106.9/1,000 copies, $P = 0.015$, Mann–Whitney) among cases positive for HLA-A*2402 but not A*0201.

proviral load. Therefore, previous reports have focused on the 'efficiency' of the CTL response as a factor of reduction in the proviral load rather than the frequency of specific CTLs, which was considered an unreliable index of the effectiveness of the CTL response [Bangham, 2003]. In fact, both experiment [Ogg et al., 1998; Kubota et al., 2000; Wodarz and Bangham, 2000; Betts et al., 2001; Wodarz et al., 2001] and theory [Bangham, 2002; Addo et al., 2003] have shown various results indicating positive, negative, or zero correlations between the specific CTL frequency and virus load. In support of this idea, the frequency of Tax11-19-specific CTLs was significantly lower than that of Tax301-309-specific CTLs in the present study (Fig. 4). However, the higher frequency of Tax301-309-specific CTLs also showed a negative relationship to the proviral load after exclusion of the bias due to Tax11-19-specific CTLs (Fig. 6). As Tax301-309-specific CTLs may make a weaker CTL response to HTLV-1 than Tax11-19-specific CTLs, these CTLs may have to proliferate more frequently to reduce the proviral load sufficiently. The results of the present study demonstrate that a high frequency of Tax-specific CTLs can maintain a relatively low HTLV-1 proviral load and can be a factor in reduction of the proviral load in healthy carriers in addition to 'CTL efficiency'.

However, the present study had the limitation that our method can detect only HTLV-1-specific $CD8^+$ cells possessing either HLA-A*0201 or A*2402. Although more than 80% of HTLV-1 carriers in the population of Southern Kyushu had HLA-A*02 or A*24, other HLA class I haplotype-restricted CTLs should be analyzed to gain a greater understanding of the whole immunity against HTLV-1 Tax.

In conclusion, we report a correlation between anti-Tax antibody and the frequency of Tax-specific CTLs. Anti-Tax antibody and Tax-specific CTLs may prevent growth of HTLV-1-infected cells in carriers. In addition, higher anti-HTLV-1 antibody titer is associated with a higher HTLV-1 proviral load. Further studies are required to focus on how HTLV-1-related markers and the host immune response impact on the development of adult T-cell leukemia/lymphoma and HAM/TSP.

ACKNOWLEDGMENTS

We thank Tatsuo Kuroki of Department of Clinical Laboratory, Kagoshima University Hospital (Kagoshima, Japan), for his excellent technical assistance. This work was supported in part by a Grant-in-Aid (to N.A.; Research on Advanced Medical Technology) from the Japanese Ministry of Health, Labour, and Welfare, and by Kagoshima University for Frontier Science Research Center Program (to N.A.).

REFERENCES

Addo MM, Yu XG, Rathod A, Cohen D, Eldridge RL, Strick D, Johnston MN, Corcoran C, Wurcel AG, Fitzpatrick CA, Feeney ME, Rodriguez WR, Basgoz N, Draenert R, Stone DR, Brander C, Goulder PJ, Rosenberg ES, Altfeld M, Walker BD. 2003. Comprehensive epitope analysis of human immunodeficiency virus type 1 (HIV-1)-specific T-cell responses directed against the entire expressed HIV-1 genome demonstrate broadly directed responses, but no correlation to viral load. J Virol 77:2081–2092.

Bangham CRM. 2002. Genetics and dynamics of the immune response to HTLV-I. Gann Monogr Cancer Res 50:397–402.

Bangham CRM. 2003. The immune control and cell-to-cell spread of human T-lymphotropic virus type 1. J Gen Virol 84:3177–3189.

Bangham C, Kermode A, Hall S, Daenke S. 1996. The cytotoxic T lymphocyte response to HTLV-I: The main determinant of disease? Semin Virol 7:41.

Bangham CR, Hall SE, Jeffery KJ, Vine AM, Witkover A, Nowak MA, Wodarz D, Usuku K, Osame M. 1999. Genetic control and dynamics of the cellular immune response to the human T-cell leukaemia virus, HTLV-I. Philos Trans R Soc Lond B Biol Sci 354:691–700.

Betts MR, Ambrozak DR, Douek DC, Bonhoeffer S, Brenchley JM, Casazza JP, Koup RA, Picker LJ. 2001. Analysis of total human immunodeficiency virus (HIV)-specific $CD4^+$ and $CD8^+$ T-cell responses: Relationship to viral load in untreated HIV infection. J Virol 75:11983–11991.

Biddison WE, Kubota R, Kawanishi T, Taub DD, Cruikshank WW, Center DM, Connor EW, Utz U, Jacobson S. 1997. Human T cell leukemia virus type I (HTLV-I)-specific $CD8^+$ CTL clones from patients with HTLV-I-associated neurologic disease secrete proinflammatory cytokines, chemokines, and matrix metalloproteinase. J Immunol 159:2018–2025.

Bieganowska K, Hollsberg P, Buckle GJ, Lim DG, Greten TF, Schneck J, Altman JD, Jacobson S, Ledis SL, Hanchard B, Chin J, Morgan O, Roth PA, Hafler DA. 1999. Direct analysis of viral-specific CD8+ T cells with soluble HLA-A2/Tax 11-19 tetramer complexes in patients with human T-lymphotropic virus-associated myelopathy. J Immunol 162:1765–1771.

Daenke S, Kermode AG, Hall SE, Taylor G, Weber J, Nightingale S, Bangham CR. 1996. High activated and memory cytotoxic T-cell responses to HTLV-1 in healthy carriers and patients with tropical spastic paraparesis. Virology 217:139–146.

Ehrlich G, Greenberg S, Abbot M. 1990. Detection of human T-cell lymphoma/leukemia viruses. In: Innis M, Gelfand D, Suinsky J, White T, editors. PCR protocols. San Diego: Academic Press. pp 325–332.

Elovaara I, Koenig S, Brewah AY, Woods RM, Lehky T, Jacobson S. 1993. High human T cell lymphotropic virus type 1 (HTLV-1)-specific precursor cytotoxic T lymphocyte frequencies in patients with HTLV-1-associated neurological disease. J Exp Med 177: 1567–1573.

Etoh K, Tamiya S, Yamaguchi K, Okayama A, Tsubouchi H, Ideta T, Mueller N, Takatsuki K, Matsuoka M. 1997. Persistent clonal